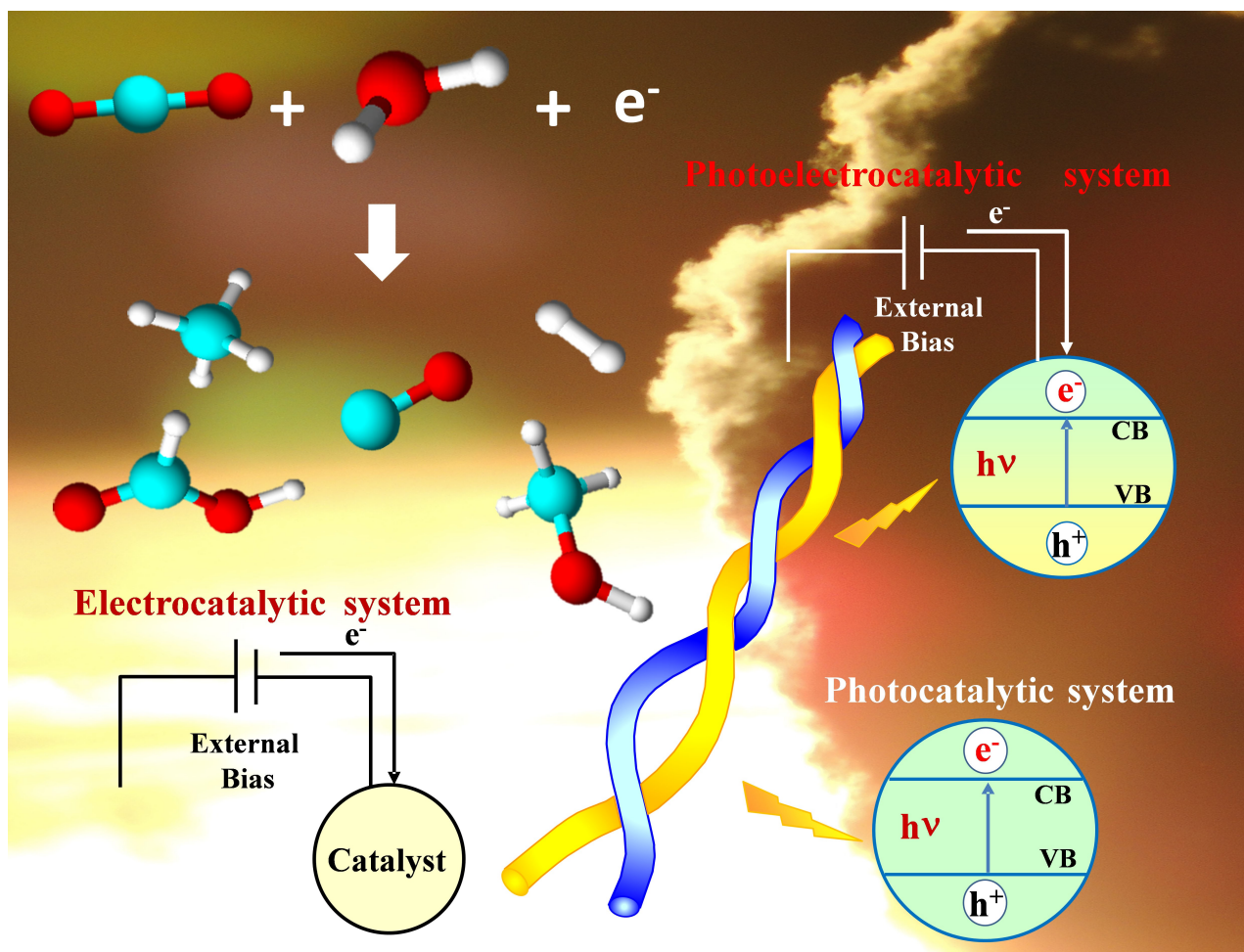


VIP Very Important Paper

Special  
Collection

# (Photo)electrocatalytic Versus Heterogeneous Photocatalytic Carbon Dioxide Reduction

Marianna Bellardita,<sup>\*[a]</sup> Vittorio Lodo,<sup>[a]</sup> Francesco Parrino,<sup>[b]</sup> and Leonardo Palmisano<sup>[a]</sup>

The present review summarizes some of the main results achieved in electrochemical, photocatalytic, and (photo)-electrocatalytic systems for the reduction of carbon dioxide. After a preliminary survey of the electrocatalytic and photocatalytic systems in terms of materials used, efficiencies, operating conditions, and product distribution, it is shown how the combination of the two approaches affords often higher efficiency than the single technologies and allows better control of the product distribution. In fact, the peculiar energetic distribution at the interface of irradiated semiconductors under opportune electrical bias enables enhancement of the spatial

separation of the photogenerated charges and minimization of the external energy required in electrochemical applications. Even though the efficiency of CO<sub>2</sub> reduction is still far away from being industrially appealing, in some cases the photoelectrocatalytic systems are promising tools to be further investigated for sustainable green chemistry based CO<sub>2</sub> utilization. The aim of this review is to examine the strengths and the weaknesses of the different approaches considering that sometimes one of the three methods can be used more successfully than the others, depending on the desired product(s) and the materials used as photocatalysts or as the (photo)electrode.

## 1. Introduction

Carbon dioxide represents the most abundant and inexpensive carbon source that can be transformed into valuable chemicals as fuels (methane, methanol, ethanol, carbon monoxide),<sup>[1–3]</sup> polymers (polycarbonates),<sup>[4,5]</sup> and valuable compounds (formic acid, carbonates) of industrial interest.<sup>[6–7]</sup> The size of the market for these compounds is around 4500 Mton per year; for this reason, the exploitation of CO<sub>2</sub> has attracted the interest of both the scientific and industrial communities, and intense efforts have been made to develop efficient conversion systems.<sup>[8]</sup> CO<sub>2</sub> transformation processes aim at artificially reproducing natural photosynthesis under mild conditions (ambient temperature and atmospheric pressure). In particular, the use of the sunlight is highly desired to perform environmentally friendly processes capable to mitigate, in a long term view, the effects of greenhouse gases and the consequent climate changes.

Various strategies of CO<sub>2</sub> valorization have been proposed such as catalytic,<sup>[9,10]</sup> photocatalytic<sup>[1,11–14]</sup> and electrocatalytic methods,<sup>[15–18]</sup> or biological processes.<sup>[19,20]</sup> Nevertheless, unfortunately, the reaction mechanism is not yet fully understood and the reported CO<sub>2</sub> conversion efficiencies are often scarce. Different types of challenges need to be faced because (i) the reactivity of CO<sub>2</sub> is low, (ii) the CO<sub>2</sub> reduction reaction is thermodynamically up-hill (CO<sub>2</sub> is a stable and thermodynamically inert compound), (iii) the catalysts used today are not very active and selective, (iv) the efficiencies of the proposed reactors are generally low, (v) the optimal experimental conditions at which the reaction should be carried out are still to be found.<sup>[21,22]</sup> Therefore, many efforts have been directed

towards the optimization of operating conditions, the search for efficient catalysts and the design of suitable reactors,<sup>[23–25]</sup> and the exploitation of solar energy as the driving force.<sup>[26,27]</sup>


Traditional thermal catalysis processes require severe reaction conditions and large amounts of energy. The photocatalytic method, although representing a very promising process because it can be carried out under mild experimental conditions and using sunlight as the radiation source, has shown some drawbacks. Among them, we mention the modest exploitation of solar energy (linked to the semiconductor band-gap), and the low efficiency due both to the high recombination rate of the photogenerated charges and to the thermodynamic limitations of CO<sub>2</sub> reduction.


A more cost-effective approach is the electrochemical conversion of CO<sub>2</sub> since electric energy can be converted directly into chemical energy. Also this technology has some drawbacks such as the need for high overpotentials, the low selectivity towards the products, and the small faradaic efficiency. The low selectivity and the high overpotentials are due to the adsorption energies of the reaction intermediates which are often significant, while the reduced faradaic efficiency is due to the competitive hydrogen evolution reaction (HER), which takes place at the same CO<sub>2</sub> reduction potential, but with a faster kinetics.<sup>[28]</sup>

The use of different approaches showing synergistic effects is a strategy to increase the efficiency of the process.<sup>[27]</sup> In particular, by coupling the photocatalytic method with the electrochemical one, the performance of the first process can be improved by applying an external potential.<sup>[29]</sup> In this way it is possible to obtain a better conversion of light into chemical energy and a higher charge separation efficiency. To improve the CO<sub>2</sub> conversion and the selectivity towards target products in a photoelectrocatalytic system, the material working as (photo)electrocatalyst (it can be used as bulk electrode or supported on a substrate working as the electrode) needs to strongly interact with CO<sub>2</sub> and to have a specific distribution of surface sites. In addition to a correct choice of the electrode, it is necessary to optimize the potential to be applied and, in general, to opportunely design the (photo)reactor.<sup>[24,26,30]</sup> It should be noted that the materials used as electrodes in the photoelectrocatalytic process can be similar and only sometimes the same as those used as catalysts in the photocatalytic and electrocatalytic ones.

[a] Prof. M. Bellardita, Prof. V. Loddo, Prof. L. Palmisano  
Engineering Department  
University of Palermo, Palermo (Italy)  
E-mail: marianna.bellardita@unipa.it

[b] Prof. F. Parrino  
Department of Industrial Engineering  
University of Trento, Trento (Italy)

 An invited contribution to a Special Collection on Photocatalytic CO<sub>2</sub> Reduction.

 © 2021 The Authors. ChemPhotoChem published by Wiley-VCH GmbH. This is an open access article under the terms of the Creative Commons Attribution License, which permits use, distribution and reproduction in any medium, provided the original work is properly cited.

In this article we will present and comment only some selected papers that report the (photo)electrocatalytic and photocatalytic reduction of CO<sub>2</sub> with the aim of qualitatively examining strengths and weaknesses of the proposed methods. It is in fact very difficult, if not impossible, to evaluate the efficiency and convenience of the various systems proposed from a quantitative point of view, since the different experimental conditions and the very low yields reported so far make the methodologies difficult to be compared.

## 2. Electrocatalysis

### 2.1. General Considerations

It is possible to convert CO<sub>2</sub> electrocatalytically into valuable compounds under mild experimental conditions directly on the surface of an electrode by applying an adequate potential and in the presence of a suitable catalyst.<sup>[31]</sup> Figure 1 shows a scheme of a cell used for the electrochemical conversion of carbon dioxide.

From a thermodynamic point of view, CO<sub>2</sub> reduction is a very challenging reaction due to its very high stability. In fact, on inert electrodes, the first step should be the one-electron direct reduction of CO<sub>2</sub> to CO<sub>2</sub><sup>•-</sup> radical anion,<sup>[32]</sup> but it is a very energy-intensive and harsh reaction ( $E^{\circ} = -1.9 \text{ V}$  for  $\text{CO}_2 + \text{e}^- \rightarrow \text{CO}_2^{\bullet-}$  in water at pH=7). The multi-electron reduction reactions, although more complex, are thermodynamically favourite, compared to one electron reduction. In fact, the free energy progressively decreases by increasing the number of

electrons needed to reduce CO<sub>2</sub> to different compounds (Figure 2).<sup>[33]</sup>

In spite of the thermodynamic trend, the most common products obtained by electrocatalytic reduction of CO<sub>2</sub> are CO, CH<sub>4</sub> and HCOOH as other factors, such as the need to overcome the kinetic limitations, play an important role. The type of material (often a metal) used as the electrode can reduce kinetics constraints while also acting as a catalyst.

Many reaction mechanisms involving heterogeneous catalysts are reported in the literature and many pathways for the same reaction are also possible in electrocatalysis. In fact, since CO<sub>2</sub> activation generally begins with its adsorption on a catalyst site, different adsorption modes and reaction mechanisms are possible on a material showing different types of active sites.<sup>[21]</sup>

### 2.2. Electrode Materials

#### 2.2.1. Single Metal Electrodes

The electrodes can consist of metals that participate in the redox process or oxides/semiconductors that can act as catalysts/photocatalysts. The process can be controlled by adjusting some operating parameters such as the type of electrode, the redox potential, the nature of the electrolytes, the pH, the temperature, the applied potential. Aqueous and non-aqueous solutions (to improve CO<sub>2</sub> solubility) or solids to suppress the H<sub>2</sub>-forming reaction are used as electrolytes.

A variety of products can be formed in aqueous solution including CO, CH<sub>4</sub>, HCOOH, CH<sub>3</sub>OH and longer chain hydrocarbons depending on the experimental conditions used. By



Marianna Bellardita graduated in 2004 in Chemical Engineering and in 2008 obtained the PhD in "Technologies and New Chemical Materials" at the University of Palermo. She is currently assistant professor at the University of Palermo. Her research activity has been mainly focussed on heterogeneous photocatalysis and involves the preparation and characterization of photocatalysts for the degradation of pollutants, green synthesis of high-value-added chemicals, CO<sub>2</sub> reduction and H<sub>2</sub> production under UV- and solar-light irradiation.



Vittorio Loddo is currently Associate Professor of Transport Phenomena at The University of Palermo. In the course of his scientific activity, he has contributed to the following fields: chemical kinetics of heterogeneous photocatalytic systems, modelling of heterogeneous photoreactors, radiation field modelling in absorbing-reacting media, advanced oxidation processes for environment remediation and green synthesis.



Leonardo Palmisano (1950) obtained his degree in Chemistry (cum Laude) in 1973 at the University of Palermo. He is Full Professor of Chemistry at the University of Palermo, Dipartimento di Ingegneria, since 01/11/2000. His scientific activity has mainly focused on the field of heterogeneous photocatalysis, such as preparation, characterization with many bulk and surface techniques, and testing of various types of bare and doped polycrystalline photocatalysts.



Francesco Parrino is an Assistant Professor of Chemistry at the University of Trento, Italy. He graduated cum laude in Chemical Engineering from the University of Palermo in 2005 and obtained a PhD in Inorganic Chemistry from the Friedrich-Alexander University of Erlangen-Nuernberg, Germany, in 2009. His research activity deals with the combination of different advanced oxidation processes and with the preparation and characterization of photocatalysts for degradation of pollutants and for green synthesis of organic molecules. His scientific interests combine mechanistic and fundamental aspects of heterogeneous photocatalysis with engineering issues for industrial applications.

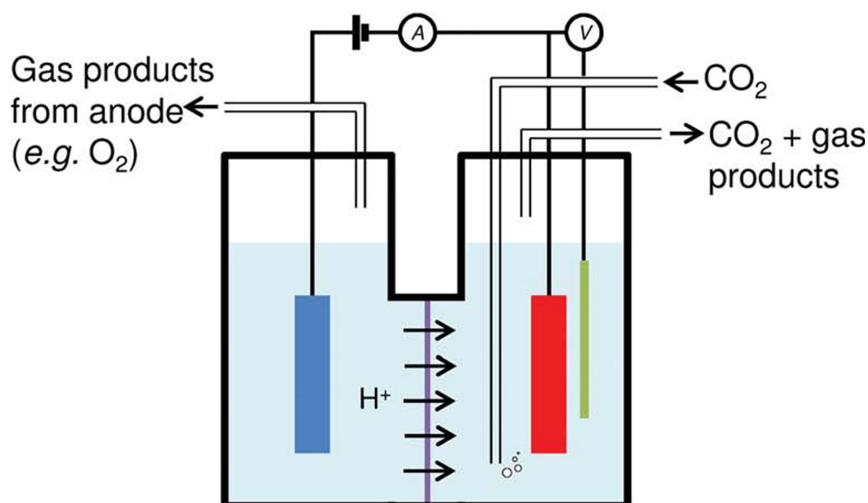


Figure 1. Scheme of a cell used for the electrochemical conversion of  $\text{CO}_2$ . Reproduced with permission from Ref. [31] Copyright (2013) Royal Society of Chemistry.

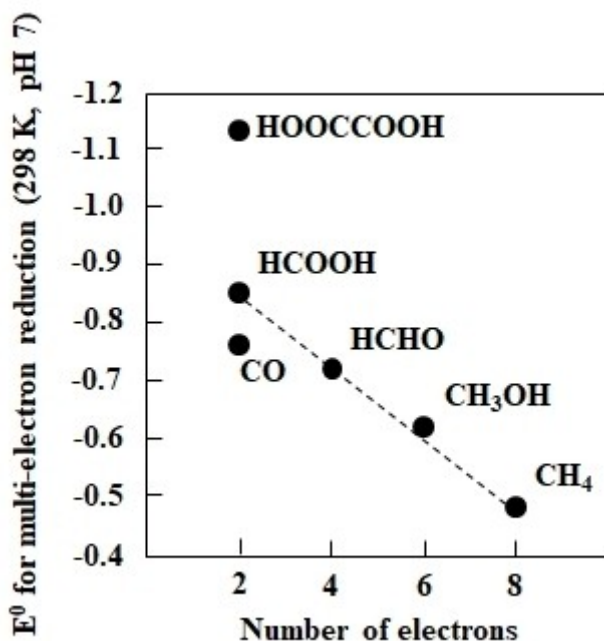


Figure 2. Reduction potential versus saturated calomel electrode versus the number of electrons necessary for the formation of the different compounds. Reproduced with permission from Ref. [33] Copyright (2002) Elsevier.

selecting the metal cathode it is possible to address the selectivity of the process. It has been reported that, for single metal cathodes, Cu, Au, Ag and Zn have shown a high selectivity towards CO; In, Pb, Sn and Cd provided formate as the main product; Ni, Fe, Pt and Ti almost exclusively produced  $\text{H}_2$ .<sup>[34]</sup> The electrolyte consisted of a 0.1 M aqueous solution of  $\text{KHCO}_3$  and the current density ranged from 0.5 to 5  $\text{mA cm}^{-2}$ .

The selectivity towards CO formation followed the series  $\text{Au} > \text{Ag} > \text{Cu} > \text{Zn} \gg \text{Cd} > \text{Sn} > \text{In} > \text{Pb} > \text{Ti} \approx \text{Hg}$  (Table 1) and depended on the ability of  $\text{CO}_2^{* -}$  to adsorb on the cathode

surface. In particular, CO was obtained from strongly adsorbed  $\text{CO}_2^{* -}$  while  $\text{HCOO}^-$  from free or weakly adsorbed  $\text{CO}_2^{* -}$ . In the latter case the carbon atom of desorbed  $\text{CO}_2^{* -}$  was protonated to formate ion. Formic acid can be obtained in acidic medium. Multimetal cathodes showed variable selectivity towards CO and  $\text{HCOO}^-/\text{HCOOH}$ , which was influenced by the combination of the electrode components, in particular the metal acting as a substrate and the metal acting as a modifier.

Nguyen et al.<sup>[35]</sup> selectively obtained CO on porous nanostructured Zn electrocatalysts with a faradaic efficiency of 78.5% and 95.3% in the presence of aqueous solution of 0.5 M  $\text{KHCO}_3$  and 0.5 M KCl as the electrolytes, respectively. X-ray photoelectron spectroscopy (XPS) measurements on the electrodes revealed that oxidized zinc states were the active sites for electrochemical  $\text{CO}_2$  reduction and that high amounts of oxidized Zn inhibited carbon deposition on the electrode surface. Adsorption of halides on Zn electrodes improved the process performance and inhibited the hydrogen formation by increasing the Faraday efficiency up to 97%.<sup>[36]</sup> Similar results were obtained by other researchers.<sup>[37–43]</sup>

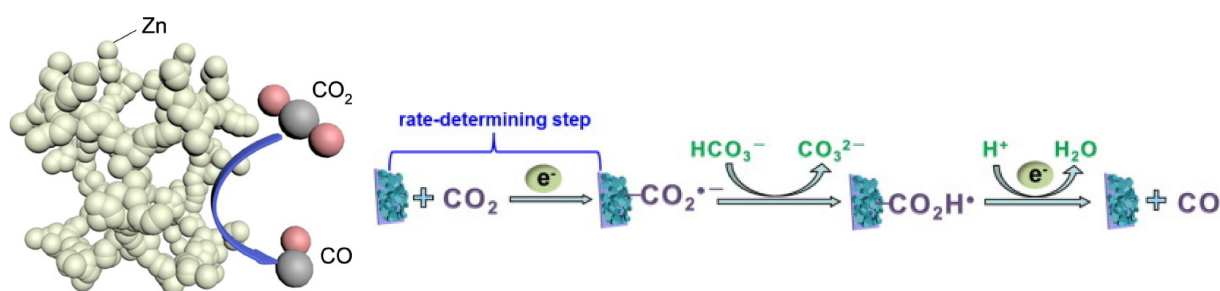
Figure 3 shows the pathway of the formation of CO from  $\text{CO}_2$ . A drawback of bulk Zn electrodes was the possibility of its oxidation after contact with water or air, moreover also the morphology and the structure have a strong influence on their efficiency. By modifying the morphology it was possible to increase and tune the activity and selectivity of the Zn-based electrodes as the exposure of their surface active sites was modified.

Formate was obtained as the main product on Zn electrodes with a particular morphology.<sup>[44,45]</sup> Yadav et al.<sup>[44]</sup> obtained, in fact, this ion with a maximum faradaic efficiency of 78.46% in the presence of an electrocatalyst consisting of Zn nanoparticles deposited on graphite plates.

Zhang et al.<sup>[45]</sup> used a Zn electrode with a nanoparticle layer as a harmless and cheap alternative to Pb and Hg for the efficient formation of formate in aqueous solution. A faradaic

**Table 1.** Main products formed during the CO<sub>2</sub> electrocatalytic reduction on different metal electrodes. Electrolyte: 0.1 M KHCO<sub>3</sub>; temperature: 18.5 °C. Reproduced with permission from Ref. [34] Copyright (1994) Elsevier.

Electrode	Potential [V] versus NHE	Faradaic efficiency [%]			
		CH <sub>4</sub>	CO	HCOO <sup>-</sup>	H <sub>2</sub>
Cu	-1.44	33.3	1.3	9.4	20.5
Au	-1.14	-	87.1	0.7	10.2
Ag	-1.37	-	81.5	0.8	12.4
Zn	-1.54	-	79.4	6.1	9.9
Pd	-1.20	2.9	28.3	2.8	26.2
Ga	-1.24	-	23.2	-	79.9
Pb	-1.63	-	-	97.4	5.0
Hg	-1.51	-	-	99.5	-
In	-1.55	-	2.1	94.9	3.3
Sn	-1.48	-	7.1	88.4	4.6
Cd	-1.63	1.3	13.9	78.4	9.4
Tl	-1.60	-	-	95.1	6.2
Ni	-1.48	1.8	-	1.4	88.9
Fe	-0.91	-	-	-	94.8
Pt	-1.07	-	-	0.1	95.7
Ti	-1.60	-	-	-	99.7

**Figure 3.** Schematic pathway for the electrocatalytic CO<sub>2</sub> reduction to CO on the surface of a Zn electrode. Reproduced with permission from Refs. [38] and [43], both copyright (2018) Elsevier.

efficiency over 87% was obtained. The figure above was more significant than those found using a bulk Zn sheet as an electrode. The good performance was attributed to the high surface area and the type of active exposed facets.

Cu electrodes have been used extensively not only because Cu has been shown to be highly efficient in forming hydrocarbons with good faradaic efficiency, but also because of the observed high reaction rates.<sup>[46–56]</sup> The reported formed products included methane, methanol, formaldehyde and formic acid, depending on the morphology of the electrode, the oxidation state of the Cu and the experimental conditions under which the experiments were carried out, such as the type of solvent, electrolyte and applied bias.

Frese et al.<sup>[49]</sup> obtained CH<sub>3</sub>OH as a direct product of the electrochemical reduction of CO<sub>2</sub> with high current densities (up to 33 mA cm<sup>-2</sup>) and yield close to 100% in the presence of oxidized Cu electrodes, 0.5 M KHCO<sub>3</sub>, pH=7.6, and -1.9 V (SCE). H<sub>2</sub> and small amounts of CO were also formed.

A mixture consisting mainly of CO and HCOOH (faradaic efficiency 21.5% and 20.2%, respectively), with small amounts of CH<sub>3</sub>OH (faradaic efficiency around 1–2.5%) was obtained with a Cu (core)/CuO (shell) catalyst<sup>[47]</sup> in a flow reactor and 1 M KHCO<sub>3</sub> aqueous solution as the electrolyte. A change in the oxidation state of Cu from Cu(0) to Cu(I) and Cu(II) was observed by changing the applied potential, and the total

faradaic efficiency for CO, HCOOH and CH<sub>3</sub>OH was greater when the cathodic potential was more negative, reaching 42.7% at -1.73 V. The presence of the different oxidation states of Cu favoured the adsorption of protons and the formation of complex products. Le et al.<sup>[50]</sup> performed the reduction of CO<sub>2</sub> to CH<sub>3</sub>OH on thin films of electrodeposited cuprous oxide with a production up to 43 μmol h<sup>-1</sup> and faradaic efficiencies up to 38%, and the values were higher than those obtained with air and oxidized or anodized Cu electrodes. These results suggest that Cu(I) played a crucial role in addressing selectivity towards CH<sub>3</sub>OH. Also in this case the copper exhibited different oxidation states after the reaction and the yield in methanol depended on the Cu(I) concentration.

Electrochemical impedance spectroscopy was used to study the mechanism of the CO<sub>2</sub> reduction reaction and to shed light on adsorption/desorption steps of the reduction intermediates.<sup>[57]</sup> The adsorption of the electroactive species on the electrode surface started at -0.13 V and the critical bias for the beginning of the charge transfer to the species adsorbed was -0.31 V. The formation of the products was related to the pH near the electrode surface, to the adsorption of HCO<sub>3</sub><sup>-</sup> and CO<sub>3</sub><sup>2-</sup> and to the applied potential. The first step is the formation of CO<sub>2</sub>\*- which can be further reduced to form HCOO<sup>-</sup>, CO, CH<sub>4</sub>, and C<sub>2</sub>H<sub>4</sub> in successive stages (Figure 4). The

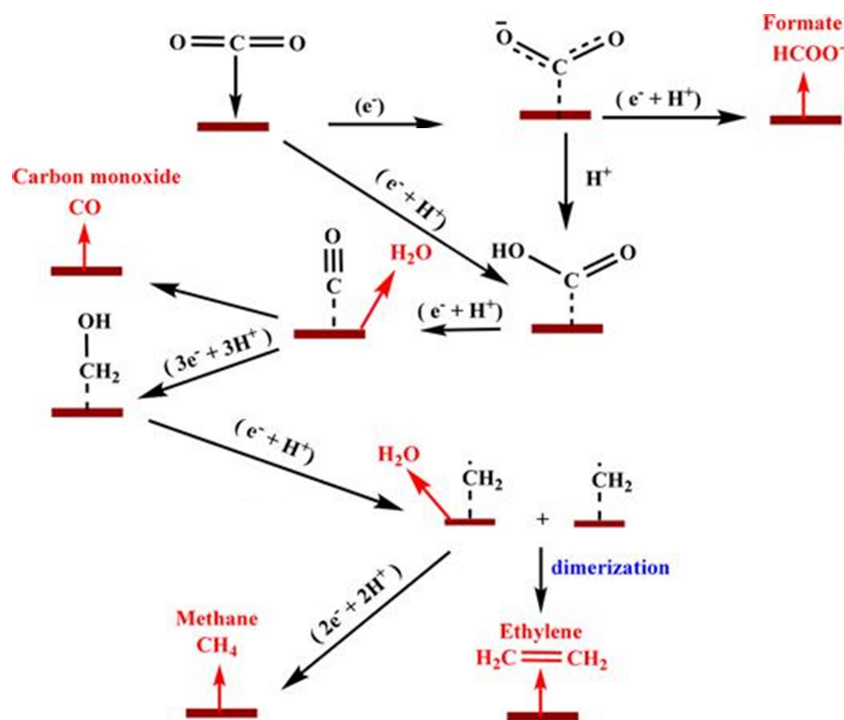


**Figure 4.** Hypothesized mechanisms for the formation of formate, CO, CH<sub>4</sub>, and C<sub>2</sub>H<sub>4</sub>. Reproduced with permission from Ref. [57] Copyright (2018) American Chemical Society.

\*COOH\* intermediate (adsorbed on the catalyst surface) proved, instead, to be the key intermediate for the production of C<sub>2</sub> and C<sub>3</sub> products which proceeded via the formation of enol-like surface intermediates.<sup>[57]</sup>

The morphology of the electrodes surface is another key parameter addressing the selectivity. It has been reported that in the presence of monocrystalline Cu electrodes ethylene formed mainly on the Cu(100) surface while methane was the main product on Cu(111) terraces.<sup>[58,59]</sup>

Investigations using other metal electrodes (Au,<sup>[60–62]</sup> Ag,<sup>[63–66]</sup> Sn<sup>[70–72]</sup>) showed similar results. The main products deriving from CO<sub>2</sub> reduction were CO and HCOOH, and their distribution depended on the structural parameters of the electrodes such as morphology and surface roughness.<sup>[73]</sup>

Notably, non-noble metals are preferable to noble metals as they are cheaper and can be used for large-scale applications (Table 2).

### 2.2.2. Multicatalyst Electrodes

Single metal electrodes that also work as catalyst have often shown low efficiency and yield due to thermodynamic limitations. The use of multi catalysts electrodes overcomes these difficulties and allows the formation of highly reduced compounds thanks to the synergism between the different components.

Cu<sub>2</sub>O/ZnO electrodes with different weight ratios were tested in continuous mode in a filter-press electrochemical cell using 0.5 M KHCO<sub>3</sub> aqueous solution as the electrolyte.<sup>[76]</sup>

Methanol was one of the main products with a maximum faradaic efficiency of 17.7% at an applied potential of –1.3 V. The coupled electrodes were more stable than those composed of a single component. The good activity was ascribed to the synergism existing between the two oxides, and in particular the formation of methanol has been attributed to the presence of Cu(I).

The incorporation of Ag into the dendritic structure of Cu with the formation of bimetallic foams of AgCu, allowed a significant decrease in the overpotential necessary to produce CO with respect to bulk silver and an increase in selectivity.<sup>[77]</sup> The maximum faradaic efficiency was 58.4% at –0.6 V on a 50/50 Ag/Cu cathode. In addition, the foams proved stable for a long time and therefore could be used in potential industrial applications. The improved activity was due to the easy desorption of CO from the surface of the AgCu bimetal electrode.

The performances of three tandem electrodes consisting of Cu/Ag, Cu/Au and Cu/Ni–N–C containing a nickel-nitrogen-metal structures (exhibiting different active sites), were compared in a flow cell operating under constant cell voltages.<sup>[78]</sup> C<sub>2</sub> (C<sub>2</sub>H<sub>4</sub> or C<sub>2</sub>H<sub>5</sub>OH) compounds were obtained from CO<sub>2</sub> reduction with high faradaic efficiency and production rate due to a reaction occurring on two adjacent catalyst layers. The first step was the CO formation while the second one the C–C coupling. The tandem electrodes displayed lower onset potential and higher partial current densities with respect to the Cu single electrode, and the best results were obtained with the Cu/Ni–N–C electrode which gave a faradaic efficiency of 62% with a partial current density of 415 mA cm<sup>–2</sup> at –0.70 V.

**Table 2.** Electrocatalytic CO<sub>2</sub> reduction efficiency from some recent literature.

Electrode	Electrolyte	Selectivity (Products)	Faradaic Efficiency [%]	Potential [V]	Ref.
Nanostructured Zn	0.5 M KHCO <sub>3</sub>	CO	78.5	−0.90 vs RHE	[35]
	0.5 M KCl		95.3	−1.05 vs RHE	
Zn nanosheets	0.5 M NaHCO <sub>3</sub>	CO	86.0	−1.13 vs RHE	[38]
Zn porous network	0.5 M NaHCO <sub>3</sub>	CO	80	−1.1 V vs RHE	[43]
Zn	0.5 M KHCO <sub>3</sub>	HCOOH	78.5	1.5 V vs RHE	[44]
	0.5 M H <sub>2</sub> CO <sub>3</sub>		38.2		
	0.5 M NaHCO <sub>3</sub>		23.2		
Cu	0.5 M NaHCO <sub>3</sub>	CH <sub>3</sub> OH	> 100	−1.9 V vs SCE	[47]
Cu(core)/CuO(shell)	0.1 M KHCO <sub>3</sub>	CO	21.5	−1.7 vs RHE	[49]
		HCOOH	20.2		
Cu nanoparticles	0.1 M KHCO <sub>3</sub>	Ethylene	41	−1.1 V vs RHE	[53]
		methane	20		
Mesoporous Cu	0.1 M KHCO <sub>3</sub>	C <sub>2</sub> H <sub>4</sub>	38	−1.7 vs RHE	[54]
		C <sub>2</sub> H <sub>6</sub>	46		
Cu nanoparticles	0.1 M NaHCO <sub>3</sub>	CH <sub>4</sub>	80	−1.25 vs RHE	[55]
		H <sub>2</sub>	13		
Plasma treated Cu	0.1 M KHCO <sub>3</sub>	C <sub>2</sub> H <sub>4</sub>	60	−0.90 vs RHE	[56]
Au nanoparticles	0.5 M KHCO <sub>3</sub>	CO	90	−0.67 vs RHE	[60]
Au nanoparticles 1–8 nm	0.1 M KHCO <sub>3</sub>	CO	88.6	−1.20 vs RHE	[61]
		H <sub>2</sub>	11.4		
Au nanowires	0.5 M KHCO <sub>3</sub>	CO	94	−0.35 vs RHE	[62]
Nanoporous Ag	0.5 M KHCO <sub>3</sub>	CO	92	−0.60 vs RHE	[67]
Mesostructured inverse opal Ag	0.1 M KHCO <sub>3</sub>	CO	80	−0.60 vs RHE	[68]
Nanostructured Ag	0.1 M KHCO <sub>3</sub>	CO	89	−0.80 vs RHE	[69]
Sn	0.1 M KHCO <sub>3</sub>	HCOO <sup>−</sup>	84	−1.60 vs RHE	[72]
Carbon supported Sn nanoparticles	0.45 M KHCO <sub>3</sub> + M KCl	HCOO <sup>−</sup>	70	−1.50 vs RHE	[74]
Sn/carbon paper	0.5 M KHCO <sub>3</sub>	HCOO <sup>−</sup>	80	−1.70 vs SCE	[75]

To avoid the use of noble metal particles, Li et al.<sup>[79]</sup> tested a ZnS/Zn/ZnS (S–Zn–S) sandwich nanostructure consisting of an inner core of Zn nanosheets and a porous sub-nanometer ZnS layer. The ZnS layer changed the adsorption properties of the composite but proved to be chemically inert during CO<sub>2</sub> reduction. The catalytic activity was tested in the presence of a 0.1 M KHCO<sub>3</sub> electrolyte saturated with CO<sub>2</sub> and was found to be comparable to that of noble metal catalysts, reaching 94.2% faradaic efficiency for the formation of CO at −0.8 V. Furthermore, the catalyst was stable for a long time maintaining a faradaic efficiency higher than 90% after 15 h of reaction at the same current density. Under the same experimental conditions, the faradaic efficiency of the pure zinc electrodes was only 71.9%.

Chen et al.<sup>[70]</sup> compared the activity of a Sn/SnO<sub>x</sub> electrode coupled with a Sn electrode in aqueous 0.5 M NaHCO<sub>3</sub> solution saturated with CO<sub>2</sub>. CO and HCOOH were formed selectively and the faradaic efficiency for the coupled electrodes was 4 times higher than that obtained on the bare Sn. The effect of SnO<sub>x</sub> was to stabilize CO<sub>2</sub><sup>•−</sup> radical anion. The authors were unable to establish whether the reduction occurred directly on the SnO<sub>x</sub> surface or at the interface between Sn<sup>0</sup> and SnO<sub>x</sub>, but the latter was essential for the CO<sub>2</sub> reduction because almost only H<sub>2</sub> was formed on the bare Sn electrode.

A paper in which two different catalysts were used for two related reduction and oxidation reactions was published by Yadav et al.<sup>[44]</sup> The electrochemical reduction of CO<sub>2</sub> to HCOOH was achieved using a Zn electrode for the reduction reaction and a cobalt oxide one for the oxidation of water which produced protons necessary for the formation of HCOOH. Sodium and potassium carbonates and hydrogen carbonates

were used as the electrolytes. The authors indicated that the optimal situation was observed in the presence of hydrogen carbonates at 1.5 V with a maximum faradaic efficiency of 78.5% after 5 minutes of reaction.

### 2.2.3. Metal-Supported TiO<sub>2</sub> Electrodes

TiO<sub>2</sub> is one of the most studied semiconductors to obtain the photocatalytic reduction of CO<sub>2</sub>,<sup>[80,81]</sup> therefore it has also been used as a support electrode in the electrochemical reduction of CO<sub>2</sub> in order to better understand its catalytic behaviour.

TiO<sub>2</sub> electrodes were prepared by Ma et al.<sup>[82]</sup> as a support for Ag in different quantities in the form of nanoparticles, and the role of the support was investigated. The authors performed some structural and electrochemical characterizations by which they hypothesized the reaction mechanism shown in Figure 5 where the participation of the Ti(IV)/Ti(III) pair is expected. The mechanism indicates that CO<sub>2</sub> was adsorbed on TiO<sub>2</sub> where it acquired an electron and turned into CO<sub>2</sub><sup>•−</sup>, which was stabilized at the TiO<sub>2</sub> surface, resulting in lower overvoltages. Subsequently, the CO<sub>2</sub><sup>•−</sup> radical, in the presence of water, was reduced to CO on the Ag sites. By using the Ag/TiO<sub>2</sub> electrode at 40 wt%, a faradaic efficiency of 90% was obtained with a current density of about 100 mA cm<sup>−2</sup>. Accordingly, authors attributed the good results to a synergistic effect between TiO<sub>2</sub> and Ag.

To increase the exposed surface, TiO<sub>2</sub> nanotubes where Ag nanoparticles have been deposited were prepared and tested.<sup>[83]</sup> With electrodes of this Ag/TiO<sub>2</sub> material, a better production of CO was observed than with bare Ag, and H<sub>2</sub> was

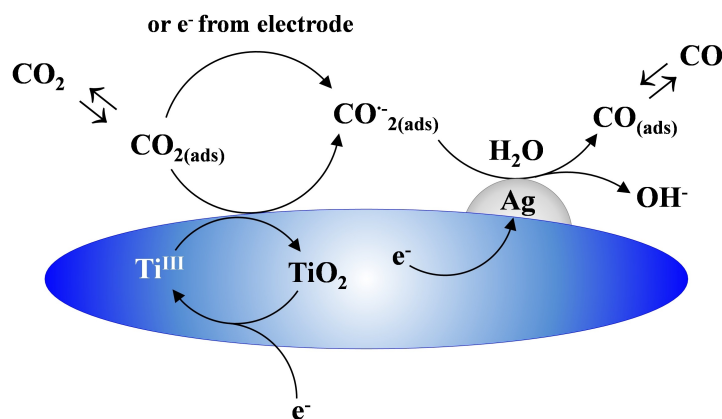


**Figure 5.** Schematic diagram of the proposed pathway for CO<sub>2</sub> reduction to CO on Ag/TiO<sub>2</sub> catalyst. Reproduced with permission from Ref. [82] Copyright (2014) John Wiley and Sons.

also formed. The results indicated that TiO<sub>2</sub> acted as a redox electron carrier to facilitate CO<sub>2</sub> reduction enhancing the stability of CO<sub>2</sub><sup>•-</sup> intermediate and the mechanism hypothesized by Ma and reported in Figure 5 was confirmed.<sup>[83]</sup>

Worthy of mention is a work describing the use of a RuO<sub>2</sub>/TiO<sub>2</sub> nanotube electrode modified with Pt which allowed the production of methanol with a current efficiency of up to 60.5%.<sup>[84]</sup>

CO<sub>2</sub> reduction was also performed on TiO<sub>2</sub> electrodes immersed in acetonitrile and very small amounts of water.<sup>[85,86]</sup> Methanol, CO and oxalate ion were obtained as the most important products. Also in this work the CO<sub>2</sub> adsorption on the catalytically active Ti<sup>3+</sup> sites with subsequent formation of the CO<sub>2</sub><sup>•-</sup> radical is proposed as the fundamental step of the reaction.

#### 2.2.4. Gas Diffusion Electrodes

Although water as a solvent is the best solution from an environmental point of view because it is the green solvent par excellence, its use also has some drawbacks. In fact, CO<sub>2</sub>, as well as H<sub>2</sub>, has a low solubility and diffusivity in water at room temperature and pressure. This leads to a decrease in current density and reaction rate due to a slow mass transfer from the bulk of the solution to the surface of the electrode. However, the CO<sub>2</sub> transfer rate can be increased by the use of pressurized electrolytes or gas diffusion electrodes (GEDs), produced with a catalyst supported on a gas diffusion layer.<sup>[30,87,88]</sup> The porous matrix of the GEDs allows the transport of gaseous CO<sub>2</sub> but limits the transport of liquids, and in addition the presence of a deposited hydrophobic layer can increase the solubility of CO<sub>2</sub> inside the electrode. By supplying gaseous CO<sub>2</sub> by means of a gas diffusion layer, current density values were measured about two orders of magnitude larger than those obtained with flat electrodes, with the same overvoltage.<sup>[89]</sup>

GEDs based on S, Ag, Sn, Zn and Cu have provided various products with efficiency depending on the electrode structure and obviously on the experimental conditions used.<sup>[74,87,90–92]</sup>

An Ag GDE was tested in three compartment cells with a current density of 150 mA cm<sup>-2</sup>. A 0.4 M K<sub>2</sub>SO<sub>4</sub> aqueous solution was used as the electrolyte and the partial pressure of CO<sub>2</sub> was adjusted to improve the recirculation of the feed. The faradaic efficiency was 60% for the conversion to CO after about 2 h.<sup>[87]</sup>

In a single, continuous pass CO<sub>2</sub> cell with a gas diffusion-supported Sn electrode, formate was formed at ambient conditions with a faradaic efficiency of 70% at 150 mA cm<sup>-2</sup>.<sup>[74]</sup>

Formate was obtained also by using a rolling Sn-loading GDE in 0.5 M KHCO<sub>3</sub> aqueous solution by applying a potential of -1.8 V. The faradaic efficiency achieved was about 79% with a current density of about 17 mA cm<sup>-2</sup>.<sup>[90]</sup>

The best performance using non-noble metals as catalysts was reported by Luo et al.<sup>[91]</sup> who compared a porous Zn electrode with a Zn GED electrode for the reduction of CO<sub>2</sub> to CO (Figure 6). For the second, the current density reached 200 mA cm<sup>-2</sup> from 27 mA cm<sup>-2</sup> at -0.64 V with a faradaic efficiency of about 84%.

#### 2.3. Hydrogen Evolution Reaction (HER) in Competition with CO<sub>2</sub> Reduction

A problem that often arises during the electrochemical reduction of CO<sub>2</sub> in the presence of aqueous electrolytes is the competitive development of hydrogen (HER).<sup>[93]</sup> In addition, there are other disadvantages such as low current density, low CO<sub>2</sub> solubility, reduced mass transfer, catalyst poisoning, and the need for separation of products from the electrolyte.

The formed H<sub>2</sub> engages the electrocatalytically active sites by consuming electrons and protons, and thus reducing the CO<sub>2</sub> conversion and the energy efficiency of the process. The choice of catalysts with high overvoltage towards H<sub>2</sub> and/or electrolytes that prevent or decrease HER, allows the achievement of high faradaic efficiencies.

Back et al.<sup>[94]</sup> compared the binding energies of \*H<sup>•</sup> (adsorbed H on the catalyst surface) at Ag and Au sites during CO<sub>2</sub> reduction. Values determined experimentally indicated that the binding energy was lower on Ag, demonstrating a



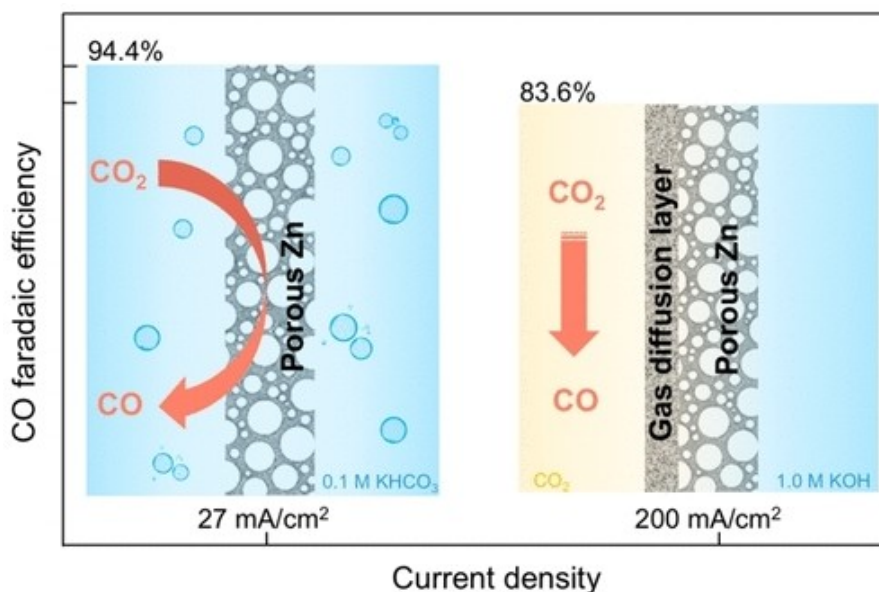


**Figure 6.** CO Faradaic efficiency versus current density in the presence of different electrode types. Reproduced with permission from Ref. [91] (<https://pubs.acs.org/doi/10.1021/acscatal.8b05109>). Copyright (2019) American Chemical Society. Further permissions related to the material excerpted should be directed to the ACS.

strong interaction of hydrogen with Au sites resulting in a more significant H<sub>2</sub> production.

It should be noted, moreover, that metal sites that interact with CO more strongly than with H<sub>2</sub> make HER competition less important as they reduce the availability of H-binding sites. Nevertheless, the interaction of the surface metal sites with CO is not the only parameter playing a role. In fact, density-functional theory (DFT) calculations indicated that, although CO adsorbs more strongly on Mo than on Cu, also the surrounding environment (e.g. the presence of co-adsorbed species) can influence the activity of the catalyst towards HER. Indeed, under the used experimental conditions, authors found a lower HER on Cu than on Mo.<sup>[93]</sup>

Moreover, the behaviour of a metal alloy can be different from that of the single components. For example, H<sub>2</sub> evolution was practically absent in an alloy of Pd and Au although Pd is a well-known effective catalyst for that reaction.<sup>[95]</sup> The experimental results indicated that by increasing the Pd content at low overpotentials (about  $-0.35$  V), the CO surface coverage underwent a noticeable increase, also competing with the adsorption of hydrogen. This finding explains the absence of H<sub>2</sub> evolution. On the other hand, bare Au exhibited poor CO<sub>2</sub> adsorption and low selectivity towards CO<sub>2</sub> reduction. Consequently, by accurately alloying different metals it was possible to increase the activity and to reduce/prevent the competitive H<sub>2</sub> production.

Goyal et al.<sup>[96]</sup> studied the competition between the reduction of CO<sub>2</sub> and the H<sub>2</sub> evolution on an Au rotating ring disk electrode. A 0.1 M hydrogen carbonate aqueous solution was used as the electrolyte and the mass transport conditions were controlled by means of the rotating ring disk electrode rate. Unexpectedly, it was found that the higher faradaic selectivity towards CO obtained in the presence of enhanced mass

transport (from 67% to 83%), was not due to the increased CO<sub>2</sub> reduction but to the hindrance of HER at the higher disk rotation rates. Water reduction was favoured at basic pH, so the improvement in mass transport depressed the HER because it reduced the pH close to the electrode.

Another strategy to prevent the H<sub>2</sub> formation was the use of solid polymer electrolytes. In these systems, CO<sub>2</sub> was fed into the catholyte compartment while the electrolyte allowed the conduction of the protons, the separation of the gaseous compounds formed, and the electrical insulation of the electrodes. Moreover, the use of solid polymer electrolyte composite electrodes enhanced the CO<sub>2</sub> mass transfer and avoided poisoning of the catalyst due to impurities in the solvent.<sup>[97–99]</sup> However, a weak point of this alternative is the faradaic efficiency lower than that obtained with electrodes in solution under similar experimental conditions.<sup>[98]</sup>

#### 2.4. Role of Solvent and Electrolyte

The faradaic efficiency of the electrocatalytic reduction of CO<sub>2</sub> depends very much on the properties of solvent and electrolyte used. In fact, solvent nature (aqueous, organic or mixed), pH, conductivity, viscosity, buffering capacity, and type of electrolyte address the distribution of the products and, therefore, the faradaic efficiency of the entire process.<sup>[100]</sup>

For example, with a Cu electrode the electrochemical reduction of CO<sub>2</sub> mainly leads to formaldehyde and methanol in aqueous medium, while CO is preferentially formed in a non-protic solvent. In fact, generally, in protic solvents a proton is transferred from the solvent to CO<sub>2</sub> adsorbed on the surface of the electrode to form hydrocarbons and/or organic compounds

containing hydrogen, whilst in aprotic solvents an oxygen is transferred from  $\text{CO}_2$  to the solvent, thus forming  $\text{CO}$ .<sup>[100]</sup>

Water is the most common solvent due to its cheapness, high availability, and environmental sustainability, but, as already highlighted, its use has some drawbacks. The faradaic efficiency is, in fact, usually low since the electrolysis of water occurs more easily over that of  $\text{CO}_2$  on the majority of transition metals used as catalysts.

In the presence of non-aqueous solvents, HER is generally absent, the solubility of  $\text{CO}_2$  is greater, and  $\text{C}_2$  compounds with high added value such as oxalate can be formed. On the other hand, organic solvents are more expensive and almost always toxic and polluting; it must also be considered that  $\text{CO}_2$  reduction requires a greater overpotential in the absence of a proton source.<sup>[101,102]</sup>

Commonly used electrolytes are hydrogen carbonates, hydroxides, alkaline cations and some anions such as halides. The type and charge of the ions also influence the  $\text{CO}_2$  reduction rate,<sup>[103–108]</sup> due to their specific adsorption and the more or less strong interaction with the electrode surface. It is therefore necessary to make a careful and thoughtful choice.

In some cases, mixed solvents have been used, generally organic compounds with the addition of water, often in small quantities, to benefit from the advantage of the presence of both.<sup>[109–114]</sup> For example, the presence of little amounts of water in acetonitrile decreased the overvoltage, increased the current density values, and accelerated the reduction of  $\text{CO}_2$  by providing protons and facilitating the formation of reaction intermediates (Figure 7).<sup>[110]</sup>

### 3. Heterogeneous Photocatalysis

$\text{CO}_2$  reduction can occur on the surface of an irradiated photocatalyst due to the formation of electrons. Since the energy gap between the LUMO and HOMO  $\text{CO}_2$  orbitals is high

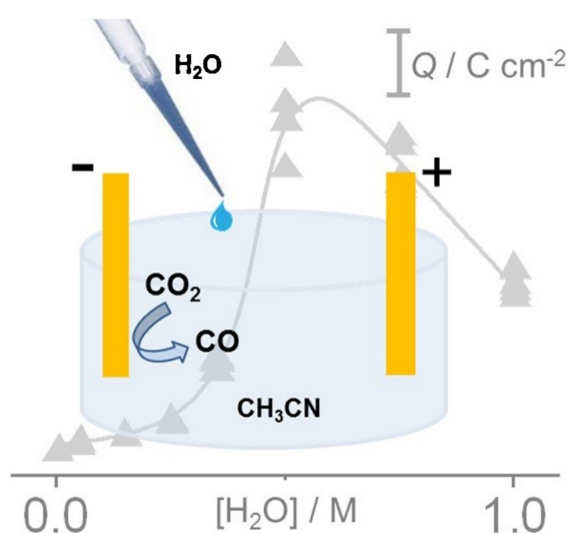


Figure 7. Effect of  $\text{H}_2\text{O}$  addition to acetonitrile on the current density. Reproduced with permission from Ref. [110] Copyright (2016) Elsevier.

(13.7 eV), the reaction is thermodynamically not favoured, and the redox potential related to the formation of radical species has the very negative value of  $-1.9\text{ V}$  (at pH 7). However, the photocatalytic method is more favoured by a thermodynamic point of view with respect to the electrochemical one. In fact, the first step of  $\text{CO}_2$  reduction is the formation of the  $\text{CO}_2^{\bullet-}$  radical by an electron transfer to its LUMO orbital. The adsorption of  $\text{CO}_2$  on the surface of the photocatalyst induces a decrease in the LUMO level of  $\text{CO}_2$ . For example, a lowering of the threshold energy of 1.4 eV above the minimum of its conduction band has been reported in the presence of  $\text{TiO}_2$ .<sup>[115]</sup>

Pioneering reports on the photocatalytic reduction of  $\text{CO}_2$  were published in the late 1980s and early 1990s.<sup>[116–122]</sup> Subsequently, a great deal of work was done and many manuscripts appeared. Various strategies have been followed with the aim of making the best use of sunlight and arriving at a competitive process as regards the conversion and selectivity towards compounds with high added value. For this purpose, various bare and doped/coupled photocatalysts have been tested both in liquid-solid and gas-solid systems with very different results.<sup>[31,123–127]</sup> The semiconductors that have been most frequently used are metal oxides. Among these we mention  $\text{TiO}_2$ ,<sup>[128–130]</sup> oxysalts as titanates, tungstate, tantalates and vanadates, metal sulphides, metal nitrides, graphitic carbon nitride, metal organic frameworks, and graphene-based systems.<sup>[69,131–136]</sup> A variety of products have been obtained depending both on the photocatalyst and on experimental conditions chosen.

It is worth noting that the presence of foreign species in a semiconductor used as a photocatalyst or the coupling of different semiconductors can improve productivity and can address the reaction towards different products than those obtained with the bare photocatalyst.<sup>[129,137]</sup> Table 3 shows some results obtained for  $\text{CO}_2$  reduction with the most representative photocatalytic systems that can be found in literature.

First, results related to a bare semiconductor ( $\text{TiO}_2$ ) were compared in analogy to bare metal electrodes. Then, metal species doped  $\text{TiO}_2$  photocatalysts were described, considering the same metals used as electrodes in the electrochemical process. Finally, some coupled photocatalytic systems were analyzed in analogy to multi catalyst electrodes. It is difficult to follow the same order for electrocatalysis and photocatalysis as the two processes are based on different working conditions; for example metals or some oxides can be used alone as electrodes and as modifiers for photocatalysts.

#### 3.1. Bare and Doped $\text{TiO}_2$ -Based Photocatalysts

The reduction of  $\text{CO}_2$  adsorbed on the surface of the powdered semiconductor chosen as photocatalyst occurs, from the thermodynamic point of view, if the edges of the valence (VB) and conduction (CB) bands of the latter are compatible with the redox potentials of the target species. Although  $\text{TiO}_2$  meets this requirement, results have not yet been exciting (Table 3).

**Table 3.** Some representative photocatalytic CO<sub>2</sub> reduction systems.

Photocatalyst	Photocatalyst precursor	Light source	Conditions	Main products	Production	Ref.
TiO <sub>2</sub> , anatase	Commercial	UV (350 nm)	H <sub>2</sub> O solution	CH <sub>4</sub>	0.88 μmol h <sup>-1</sup> g <sup>-1</sup>	[138]
TiO <sub>2</sub> pellets extruded from Degussa P25	Commercial	UVC (254 nm)	2-propanol H <sub>2</sub> O solution	CH <sub>4</sub>	2.16 μmol h <sup>-1</sup> g <sup>-1</sup>	[139]
Mesoporous TiO <sub>2</sub> nanofibers	Ti(OC <sub>4</sub> H <sub>9</sub> ) <sub>4</sub>	UVA (365 nm)	Gas phase (CO <sub>2</sub> bubbled in H <sub>2</sub> O)	CH <sub>4</sub>	95 μmol h <sup>-1</sup> L <sup>-1</sup>	[140]
Degussa P25	Commercial	UV/vis (300 W Xe arc lamp)	Gas phase (wet CO <sub>2</sub> )	CH <sub>4</sub>	47 μmol h <sup>-1</sup> L <sup>-1</sup>	[140]
TiO <sub>2</sub> , anatase particles with different size	Ti(OC <sub>4</sub> H <sub>9</sub> ) <sub>4</sub>	UVC (254 nm)	NaOH solution	CH <sub>4</sub>	19.55 μmol h <sup>-1</sup> g <sup>-1</sup>	[141]
				H <sub>2</sub>	0.78 μmol h <sup>-1</sup> g <sup>-1</sup>	[141]
				CH <sub>3</sub> OH	0.06 μmol h <sup>-1</sup> g <sup>-1</sup>	[141]
				CO	0.40 μmol h <sup>-1</sup> g <sup>-1</sup>	[141]
				CO	0.04 μmol h <sup>-1</sup> g <sup>-1</sup>	[141]
Anatase TiO <sub>2</sub> with exposed {001} and {101} facets	Ti(OC <sub>4</sub> H <sub>9</sub> ) <sub>4</sub>	300 W Xe lamp	NaHCO <sub>3</sub> solution	CH <sub>4</sub>	0.05 μmol h <sup>-1</sup> g <sup>-1</sup>	[142]
Carbon nanofibers supported TiO <sub>2</sub> , anatase {001}/(101)	Ti(OC <sub>4</sub> H <sub>9</sub> ) <sub>4</sub>	simulated sunlight irradiation	Liquid H <sub>2</sub> O	CO	1.35 μmol h <sup>-1</sup> g <sup>-1</sup>	[143]
				CO	0.6 μmol h <sup>-1</sup> g <sup>-1</sup>	[143]
Rutile TiO <sub>2</sub> modified anatase	Treated Degussa P25	300 W Hg lamp	Gas phase (wet CO <sub>2</sub> )	CH <sub>4</sub>	2.5 μmol h <sup>-1</sup> g <sup>-1</sup>	[144]
TiO <sub>2</sub> , anatase				CH <sub>4</sub>	1.3 μmol h <sup>-1</sup> g <sup>-1</sup>	[144]
Anatase TiO <sub>2</sub>				CH <sub>4</sub>	33.7 μmol h <sup>-1</sup> g <sup>-1</sup>	[145]
Anatase/Rutile TiO <sub>2</sub>	Commercial	UV/visible	NaHCO <sub>3</sub> /isopropanol	CH <sub>4</sub>	14.3 μmol h <sup>-1</sup> g <sup>-1</sup>	[145]
Degussa P25	Commercial	450 W Hg lamp		CH <sub>4</sub>	3.51 μmol h <sup>-1</sup> g <sup>-1</sup>	[145]
Oxygen-deficient TiO <sub>2</sub> :	[CH <sub>3</sub> CH(O)-CO <sub>2</sub> NH <sub>4</sub> ] <sub>2</sub> Ti(OH) <sub>2</sub>	150 W solar simulator	Gas phase (wet CO <sub>2</sub> )	CH <sub>4</sub>	10 μmol h <sup>-1</sup> g <sup>-1</sup>	[146]
Anatase	TiCl <sub>4</sub>			CH <sub>4</sub>	3.5 μmol h <sup>-1</sup> g <sup>-1</sup>	[146]
Rutile	[CH <sub>3</sub> CH(O)-CO <sub>2</sub> NH <sub>4</sub> ] <sub>2</sub> Ti(OH) <sub>2</sub>			CH <sub>4</sub>	17 μmol h <sup>-1</sup> g <sup>-1</sup>	[146]
Brookite				CH <sub>4</sub>		[146]
NaOH modified TiO <sub>2</sub>	Commercial anatase	300 W Xe lamp	Gas phase (wet CO <sub>2</sub> )	CH <sub>4</sub>	8.7 μmol h <sup>-1</sup> g <sup>-1</sup>	[147]
Cu/TiO <sub>2</sub>	Commercial	Xe lamp	Liquid H <sub>2</sub> O	CH <sub>4</sub>	0.65 μmol h <sup>-1</sup> g <sup>-1</sup>	[148]
				C <sub>2</sub> H <sub>4</sub>	0.92 μmol h <sup>-1</sup> g <sup>-1</sup>	[148]
				C <sub>2</sub> H <sub>6</sub>	0.13 μmol h <sup>-1</sup> g <sup>-1</sup>	[149]
Degussa P25 Cu-doped TiO <sub>2</sub>	Commercial	UVA	1 M KHCO <sub>3</sub>	CH <sub>3</sub> OH	443 μmol h <sup>-1</sup> g <sup>-1</sup>	[149]
				CH <sub>3</sub> OH	135 μmol h <sup>-1</sup> g <sup>-1</sup>	[149]
				CH <sub>4</sub>	1.5 μmol h <sup>-1</sup> g <sup>-1</sup>	[150]
				CO	7.5 μmol h <sup>-1</sup> g <sup>-1</sup>	[150]
				CO	100 μmol h <sup>-1</sup> g <sup>-1</sup>	[151]
Cu/TiO <sub>2</sub>	Ti(OC <sub>4</sub> H <sub>9</sub> ) <sub>4</sub>	UVC (254 nm)	0.2 N NaOH	CH <sub>3</sub> OH	25 nmol h <sup>-1</sup> g <sup>-1</sup>	[151]
Cu/TiO <sub>2</sub>	Ti(OC <sub>4</sub> H <sub>9</sub> ) <sub>4</sub>	UVA	Gas phase (wet CO <sub>2</sub> )	CH <sub>4</sub>	0.25 μmol h <sup>-1</sup> g <sup>-1</sup>	[152]
Cu/TiO <sub>2</sub>	TiCl <sub>4</sub>	UVA	Gas phase (wet CO <sub>2</sub> )	HCHO	0.52 μmol h <sup>-1</sup> g <sup>-1</sup>	[130]
Cu/TiO <sub>2</sub>	Ti(OC <sub>4</sub> H <sub>9</sub> ) <sub>4</sub>	UVA	Gas phase (wet CO <sub>2</sub> )	CH <sub>4</sub>	45 μmol h <sup>-1</sup> g <sup>-1</sup>	[153]
Cu/TiO <sub>2</sub> , supported on a Nafion membrane	Commercial	150 W solar simulator	Gas phase (wet CO <sub>2</sub> )	CO	1.1 μmol h <sup>-1</sup> g <sup>-1</sup>	[154]
Cu/TiO <sub>2-x</sub> (NaOH treated P25)	TiCl <sub>4</sub>	100 W Xe lamp	Gas phase (wet CO <sub>2</sub> )	CH <sub>4</sub>	221.6 ppm h <sup>-1</sup> g <sup>-1</sup>	[155]
Cu <sub>2</sub> O-TiO <sub>2</sub>	Ti[OCH(CH <sub>3</sub> ) <sub>2</sub> ] <sub>4</sub>	400 W Xe lamp	Gas phase (wet CO <sub>2</sub> )	CH <sub>4</sub>	1361 μmol h <sup>-1</sup> g <sup>-1</sup>	[156]
Pt-TiO <sub>2</sub> single crystals				CO	190 μmol h <sup>-1</sup> g <sup>-1</sup>	[156]
Pt/TiO <sub>2</sub> anatase film	Commercial Ti foil	UVA	0.1 M KHCO <sub>3</sub>	CH <sub>4</sub>	20.5 ppm h <sup>-1</sup> cm <sup>-2</sup>	[157]
Pt/deposited on Al <sub>2</sub> O <sub>3</sub> foam	Commercial PC500	UVC (254 nm)	Gas phase (wet CO <sub>2</sub> )	CH <sub>4</sub>	1.25 μmol h <sup>-1</sup> g <sup>-1</sup>	[158]
				CO	0.58 μmol h <sup>-1</sup> g <sup>-1</sup>	[158]
				H <sub>2</sub>	23.3 μmol h <sup>-1</sup> g <sup>-1</sup>	[159]
Pt/TiO <sub>2</sub> anatase nanoparticles	Ti(OC <sub>4</sub> H <sub>9</sub> ) <sub>4</sub>	500 W Xe lamp	Gas phase (wet CO <sub>2</sub> )	CH <sub>4</sub>	60.1 μmol h <sup>-1</sup> g <sup>-1</sup>	[159]
				H <sub>2</sub>	87.5 μmol h <sup>-1</sup> g <sup>-1</sup>	[159]
				C <sub>2</sub> H <sub>6</sub>	2.8 μmol h <sup>-1</sup> g <sup>-1</sup>	[159]
Cu-Pt supported on TiO <sub>2</sub> nanotubes	Commercial Ti foil	AM 1.5 solar simulator	Gas phase (wet CO <sub>2</sub> )	CH <sub>4</sub>	134 μmol h <sup>-1</sup> g <sup>-1</sup>	[160]
				C <sub>2</sub> H <sub>4</sub>	12 μmol h <sup>-1</sup> g <sup>-1</sup>	[160]
				C <sub>2</sub> H <sub>6</sub>	0.24 μmol h <sup>-1</sup> g <sup>-1</sup>	[160]
				CH <sub>4</sub>	33 μmol h <sup>-1</sup> g <sup>-1</sup>	[161]
Pt-Cu <sub>2</sub> O/TiO <sub>2</sub>	Commercial Degussa P25	220 W Xe-lamp	Gas phase (wet CO <sub>2</sub> )	CH <sub>4</sub>	8 μmol h <sup>-1</sup> g <sup>-1</sup>	[161]
				CO	25 μmol h <sup>-1</sup> g <sup>-1</sup>	[161]
				H <sub>2</sub>		[161]

Photocatalyst	Photocatalyst precursor	Light source	Conditions	Main products	Production	Ref.
Au/TiO <sub>2</sub>	Ti(OC <sub>2</sub> H <sub>5</sub> ) <sub>4</sub>	UVC (254 nm)	Gas phase (wet CO <sub>2</sub> )	CH <sub>4</sub> C <sub>2</sub> H <sub>6</sub> CH <sub>3</sub> OH HCHO	2.3 μmol h <sup>-1</sup> g <sup>-1</sup> 1.6 μmol h <sup>-1</sup> g <sup>-1</sup> 0.9 μmol h <sup>-1</sup> g <sup>-1</sup> 1.4 μmol h <sup>-1</sup> g <sup>-1</sup>	[162]
Au/TiO <sub>2</sub> Pt/TiO <sub>2</sub> In/TiO <sub>2</sub>	Ti(OC <sub>4</sub> H <sub>9</sub> ) <sub>4</sub> Ti[OCH(CH <sub>3</sub> ) <sub>2</sub> ] <sub>4</sub>	350 W Xe-lamp UVA	Gas phase (wet CO <sub>2</sub> ) Gas phase (wet CO <sub>2</sub> )	CH <sub>4</sub> CH <sub>4</sub> CH <sub>4</sub>	1.5 μmol h <sup>-1</sup> g <sup>-1</sup> 2.9 μmol h <sup>-1</sup> g <sup>-1</sup> 244 μmol h <sup>-1</sup> g <sup>-1</sup>	[163] [164]
Ag/TiO <sub>2</sub> Ag/TiO <sub>2</sub> brookite (001)/(210)	Ti(OC <sub>4</sub> H <sub>9</sub> ) <sub>4</sub> TiCl <sub>4</sub>	500 W Xe lamp 300 W Xe-lamp	Gas phase (wet CO <sub>2</sub> ) Gas phase (wet CO <sub>2</sub> )	CH <sub>3</sub> OH CH <sub>4</sub>	133 μmol h <sup>-1</sup> g <sup>-1</sup> 77 ppm h <sup>-1</sup> g <sup>-1</sup>	[165] [166]
TiO <sub>2</sub> Pt-TiO <sub>2</sub> MgO-Pt-TiO <sub>2</sub> Mesoporous CeO <sub>2</sub> -TiO <sub>2</sub> P25	Degussa P25 TiCl <sub>4</sub> Commercial	100 W Xe lamp 300 W Xe lamp	Gas phase (wet CO <sub>2</sub> ) Gas phase (wet CO <sub>2</sub> )	CO, CH <sub>4</sub> , H <sub>2</sub> CO, CH <sub>4</sub> , H <sub>2</sub> CO, CH <sub>4</sub> , H <sub>2</sub> CH <sub>4</sub>	1.2, 0.38, 2.1 μmol h <sup>-1</sup> g <sup>-1</sup> 1.1, 5.2, 33 μmol h <sup>-1</sup> g <sup>-1</sup> 0.8, 9, 8.4 μmol h <sup>-1</sup> g <sup>-1</sup> 1.8 mmol h <sup>-1</sup> g <sup>-1</sup>	[167] [168]
Au-Cu alloy/TiO <sub>2</sub> powders Au-Cu alloy/TiO <sub>2</sub> film	Commercial P25	1000 W Xe lamp	Gas phase (wet CO <sub>2</sub> )	CH <sub>4</sub> H <sub>2</sub> CH <sub>4</sub> H <sub>2</sub> CH <sub>4</sub>	0.17 mmol h <sup>-1</sup> g <sup>-1</sup> 4.7 mmol h <sup>-1</sup> g <sup>-1</sup> 32 μmol h <sup>-1</sup> g <sup>-1</sup> 19 μmol h <sup>-1</sup> g <sup>-1</sup> 286 μmol h <sup>-1</sup> g <sup>-1</sup> 2200 μmol h <sup>-1</sup> g <sup>-1</sup>	[169]]
Au@TiO <sub>2</sub> sheres@CoO mesoporous Fe-CeO <sub>2</sub>	Ti(OC <sub>4</sub> H <sub>9</sub> ) <sub>4</sub> Ce(NO <sub>3</sub> ) <sub>3</sub> ·6H <sub>2</sub> O	300 W Xe lamp 300 W Xe lamp	Gas phase (wet CO <sub>2</sub> ) Gas phase (wet CO <sub>2</sub> )	CH <sub>4</sub> CH <sub>4</sub>	13.3 μmol h <sup>-1</sup> g <sup>-1</sup> 2.9 μmol h <sup>-1</sup> g <sup>-1</sup>	[170] [171]
WO <sub>3</sub> WO <sub>3</sub> Nanosheets Hollow TiO <sub>2</sub> @g-C <sub>3</sub> N <sub>4</sub> TiO <sub>2</sub> /g-C <sub>3</sub> N <sub>4</sub>	Commercial Tungsten filaments Ti(OC <sub>4</sub> H <sub>9</sub> ) <sub>4</sub> Commercial P25	300 W Xe lamp λ > 420 nm 300 W Xe lamp λ > 420 nm UVC 254 nm	Gas phase (wet CO <sub>2</sub> ) 0.08 M NaHCO <sub>3</sub> Supercritical CO <sub>2</sub> saturated with H <sub>2</sub> O	CH <sub>4</sub> CH <sub>3</sub> OH CO CH <sub>4</sub> H <sub>2</sub>	0.09 μmol h <sup>-1</sup> g <sup>-1</sup> 1.1 μmol h <sup>-1</sup> g <sup>-1</sup> 8 μmol h <sup>-1</sup> g <sup>-1</sup> 2.7 μmol h <sup>-1</sup> g <sup>-1</sup> 8.5 μmol h <sup>-1</sup> g <sup>-1</sup> 40 μmol h <sup>-1</sup> g <sup>-1</sup>	[172] [173] [174]
Ag <sub>3</sub> PO <sub>4</sub> /g-C <sub>3</sub> N <sub>4</sub> P25	Commercial	500 W Xe lamp	Gas phase (wet CO <sub>2</sub> )	CO	45 μmol h <sup>-1</sup> g <sup>-1</sup> 5 μmol h <sup>-1</sup> g <sup>-1</sup>	[175]

Several commercial and home-prepared TiO<sub>2</sub> photocatalysts in various polymorphic forms were tested under UV and/or sunlight illumination in liquid and gas phase. Unfortunately, the productivity and selectivity were low and various types of products were found depending on the experimental conditions used (Table 3). In summary, CH<sub>4</sub> was the most abundant product under all experimental conditions, C<sub>2</sub> compounds and CH<sub>3</sub>OH were generally observed in the liquid phase, while CO was formed almost exclusively in the gas phase, sometimes together with H<sub>2</sub>. Notably, almost always the sum of CO and CH<sub>4</sub> represented more than 75% of the compounds obtained. HCOOH, CH<sub>3</sub>OH, and C<sub>2</sub>H<sub>5</sub>OH have been observed predom-

inantly in aqueous systems, and sometimes also traces of HCHO, C<sub>2</sub>H<sub>6</sub> and C<sub>2</sub>H<sub>4</sub> have been found.

The amount of products under solar light irradiation is generally significantly lower than under UV irradiation. Kóci et al.<sup>[176]</sup> compared the photocatalytic activity of bare TiO<sub>2</sub> and Ag/TiO<sub>2</sub> samples under different wavelengths (254, 365, and 400 nm). The main products (CH<sub>3</sub>OH in the liquid phase and CH<sub>4</sub> in the gas phase) were more abundant when the lamp emitting at 254 nm was used instead of that emitting at 365 nm, whilst a very scarce product formation occurred by using the lamp emitting at 400 nm (Figure 8). The higher activity of bare TiO<sub>2</sub> at lower wavelength can be explained by considering its high band gap, but the smaller value of Ag/TiO<sub>2</sub>

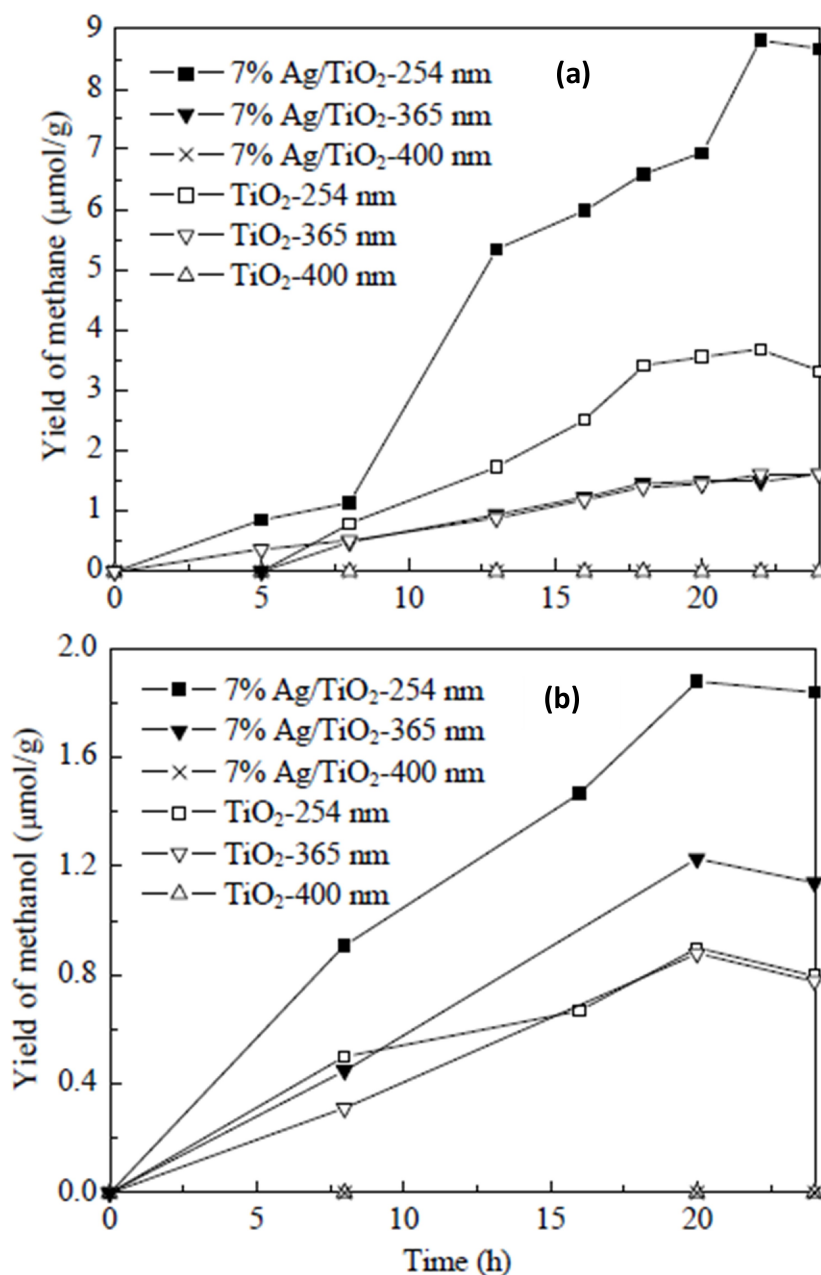


**Figure 8.** Amount of CH<sub>4</sub> (a) and CH<sub>3</sub>OH (b) versus irradiation time obtained with bare TiO<sub>2</sub> and Ag/TiO<sub>2</sub> samples under irradiation with different wavelengths. Reproduced with permission from Ref. [176] Copyright (2011) Elsevier.

band gap (2.74 eV) compared to that of bare TiO<sub>2</sub> does not justify the lower activity for Ag/TiO<sub>2</sub>. The energy levels of Ag are likely to be below the TiO<sub>2</sub> CB edge and the electrons produced by visible light do not have enough energy to reduce CO<sub>2</sub>. This represents a weakness since the use of visible light is highly desirable from the point of view of exploiting solar energy.

By examining Table 3 it can be seen that a great variety of compounds and yields have been reported in the literature using different TiO<sub>2</sub> samples, depending on the precursor used to prepare the TiO<sub>2</sub>, the phase of the latter, its morphology and the experimental conditions at which tests were carried out. The presence of metallic species, added with the aim of shifting the absorption into the visible range and to improve the separation of the photogenerated charges, did not give rise to the formation of new products but often to a different distribution of them and a greater efficiency. The metal that appears to be the most efficient is copper.<sup>[148–152]</sup> In fact, its presence induced the preferential formation of CH<sub>3</sub>OH in the liquid phase and CH<sub>4</sub> in the gaseous one. In particular, Cu<sup>+</sup> has been reported to be the most active species to produce CH<sub>3</sub>OH. Furthermore, since the XPS spectra also revealed the presence of both Cu and Cu<sup>2+</sup> species, the reduced electron/hole recombination rate was explained with the occurrence of the Cu<sup>2+</sup>/Cu<sup>+</sup> redox cycle.<sup>[149]</sup>

In order to efficiently photoreduce CO<sub>2</sub>, its adsorption on the photocatalyst surface must be favoured by increasing the surface area and the dispersion of the photocatalyst or by immobilizing the photocatalyst on inert matrices as zeolites or silicates.<sup>[179]</sup> TiO<sub>2</sub> anchored on Y-zeolite was more efficient than bulk TiO<sub>2</sub> towards CO<sub>2</sub> reduction in gas phase in the presence of H<sub>2</sub>O. The highly dispersed titanium dioxide in the zeolite cavities existed in both octahedral and tetrahedral coordination. The tetrahedrally coordinated sites were high selective towards CH<sub>3</sub>OH, whilst those octahedrally coordinated towards CH<sub>4</sub>. The observed significant activity was explained with the occurrence of the ligand-to-metal charge transfer, due to the UV light excitation of isolated Ti centers. The presence of Pt improved the charges separation and favoured the CH<sub>4</sub>

formation instead of that of CH<sub>3</sub>OH. An in-situ FT-IR spectroscopy study by Ulagappam et al.<sup>[180]</sup> during the reduction of CO<sub>2</sub> in the presence of Ti silicalite molecular sieves and methanol as sacrificial agent, indicated the presence of CO, HCOOH and CH<sub>3</sub>COOH.

Loading with metallic species<sup>[181]</sup> or inorganic modifiers (such as amino functional groups),<sup>[182,183]</sup> the addition of basic (MgO,<sup>[167]</sup> CeO<sub>2</sub>,<sup>[184]</sup> In(OH)<sub>3</sub><sup>[185]</sup>) and acidic (WO<sub>3</sub><sup>[186]</sup>) oxides, and alkali treatment of the photocatalyst<sup>[147]</sup> are other ways to improve CO<sub>2</sub> adsorption.

The CO<sub>2</sub> molecule can give rise to different modes of adsorption by interacting with the surface of the catalyst both as an electron donor and as an electron acceptor. In fact, the oxygen lone pairs allow to coordinate to the Lewis acid sites, while the carbon to the Lewis basic sites (Figure 9).<sup>[187]</sup> The various configurations justify the multiplicity of products obtained with the different photocatalysts. Consequently, research has focused on the choice of alternative catalysts to TiO<sub>2</sub> or the development of coupled systems containing both acidic and basic sites.<sup>[129,188–191]</sup>

Moreover, CO<sub>2</sub> adsorption and reaction could be improved with the introduction of oxygen vacancies.<sup>[154,192–194]</sup> Indeed, as reported by Metiu et al.<sup>[195]</sup> this type of defects enhance the Lewis basicity of the surface, and CO<sub>2</sub> molecule binds to the defective site by means of an oxygen atom which replaces the lack of oxygen. Subsequently CO<sub>2</sub> dissociates forming CO. Figure 10 schematizes the possible CO<sub>2</sub> dissociation mechanism on oxygen vacancies.<sup>[194]</sup>

In situ diffuse reflectance infrared Fourier transform spectroscopy (DRIFTS) measurements on defective Cu(I)/TiO<sub>2-x</sub> confirmed the mechanism above illustrated.<sup>[154]</sup>

CO<sub>2</sub> forms bridged-type CO<sub>2</sub><sup>-</sup> species upon interaction with the catalyst surface and electron transfer from the Ti<sup>3+</sup> sites (Figure 11 steps 1 and 2). The presence of CO bound to Cu<sup>+</sup> was explained by hypothesizing a synergistic interaction between Cu<sup>+</sup> and oxygen vacancies that weaken the O–C–O bond and induced CO<sub>2</sub> splitting. The presence of Cu<sup>+</sup> on the surface facilitated the destabilization of CO<sub>2</sub> and the use of isotopically labelled C confirmed that CO derived from CO<sub>2</sub>. The

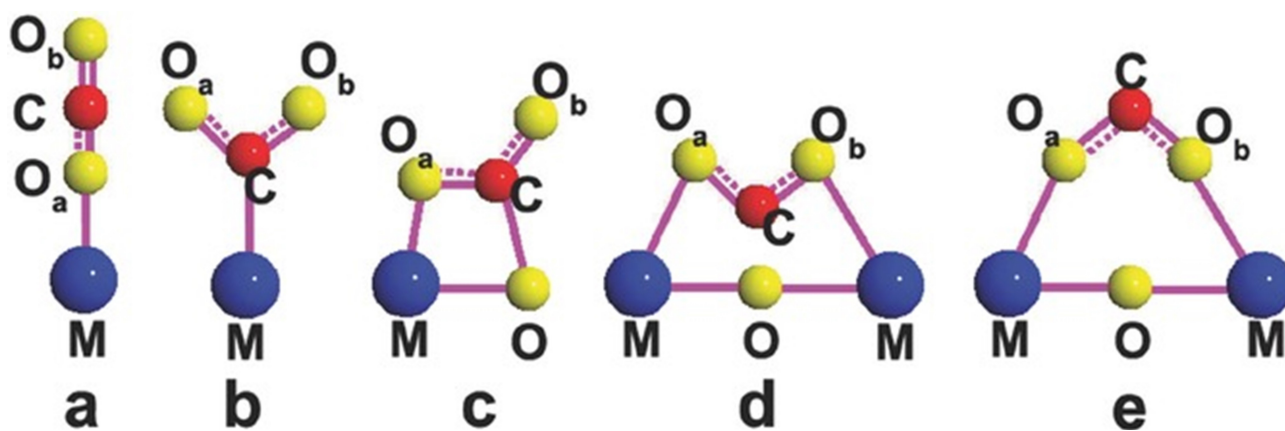


**Figure 9.** Possible CO<sub>2</sub> adsorption modes on the photocatalyst surface. M = metal species. Reproduced with permission from Ref. [187] Copyright (2014) John Wiley and Sons.

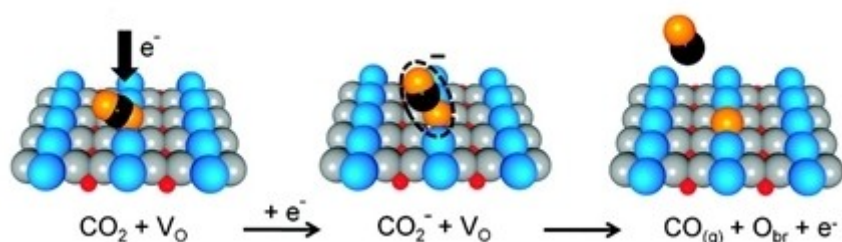


Figure 10. Possible dissociation mechanism of CO<sub>2</sub> on oxygen vacancies. Reproduced with permission from Ref. [194] Copyright (2016) American Chemical Society.

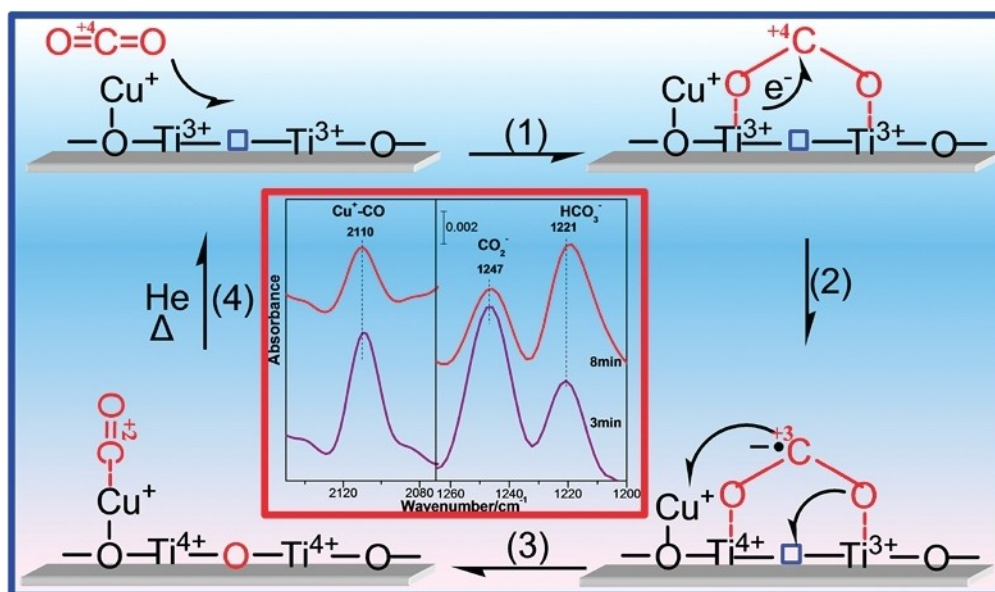


Figure 11. Hypothesized mechanism for spontaneous dissociation of CO<sub>2</sub> on Cu(I)/TiO<sub>2-x</sub> catalyst surface in the dark at room temperature. Reproduced with permission from Ref. [154] Copyright (2012) American Chemical Society.

defects consumed by CO<sub>2</sub> reduction can be easily regenerated by blowing in an inert gas at a moderate temperature. Furthermore, the oxygen vacancies have the positive effect of inducing a large light absorption capacity by the catalyst.<sup>[196]</sup>

### 3.2. Coupled TiO<sub>2</sub> and Other Photocatalysts

In addition to TiO<sub>2</sub> and the few examples reported in Table 3, numerous other bare or coupled photocatalysts have been investigated for the reduction of CO<sub>2</sub>. Among these we find several type of metal oxides, carbon based materials (carbon nitride, graphene, metal organic framework), metal sulfides, and metal nitrides.<sup>[31,69,133–135,197]</sup>

Despite the countless studies, the photocatalytic reduction of CO<sub>2</sub> could not be satisfactorily achieved as can be noticed from Table 3. Even with other more complex systems, not reported for the sake of brevity in Table 3, the quantities of formed products are of the same order of magnitude.<sup>[198–204]</sup> Just in the work of Wang et al.<sup>[168]</sup> high activity is reported not only for mesoporous CeO<sub>2</sub>-TiO<sub>2</sub> sample but also for the

commercial P25. For the latter sample the activity was much higher than that generally reported in the literature, but an error in the determination of the quantities of the products or contributions relating to the presence of impurities cannot be excluded. The low yields towards products reported by almost all works can be related not only to thermodynamic but also to kinetic hindrances. In fact, the electron-hole recombination rate (10<sup>-9</sup> s) is very fast, when compared with the time necessary for the photogenerated charges to reach the species adsorbed on the catalyst surface (10<sup>-8</sup>–10<sup>-3</sup> s).

A direct comparison of the data reported in papers published by various research groups is very difficult due to the very different experimental conditions. It is obviously assumed that different photocatalysts have different physicochemical properties, but this also happens for formally identical catalysts but prepared by different methods.<sup>[24,30,205]</sup> Furthermore, the reaction configurations such as reactor, temperature, solvent and light intensity are different and often not well specified. The intensity of the light affects not only the yield of the products but also their distribution, even if a generalization is not possible. Many reaction mechanisms are reported in

literature and they depend on the type of photocatalyst, in particular on some of its features like surface area, porosity, particle dimensions, conduction band edge potential, surface electron density, acidity-basicity, and presence of defects. It is also necessary to take into account the thermodynamics and kinetics of photoadsorption and photodesorption phenomena involving CO<sub>2</sub>, intermediate species and reduction products.

Despite intense efforts, the photocatalytic reduction of CO<sub>2</sub> is still considered inefficient. This is mainly due to the low reaction activity and selectivity towards the products, the low exploitation of sunlight, and the absence of scalable reactor designs. The main task remains the engineering of a suitable photocatalyst for the activation and efficient conversion of CO<sub>2</sub> under solar radiation.

### 3.3. Solvent and Precursor Effects

For the reactions carried out in the liquid-solid regime, water is the most used solvent, despite it has the drawback of the low solubility of CO<sub>2</sub> and the possible simultaneous formation of H<sub>2</sub>. The solubility of CO<sub>2</sub> can be increased by raising the pH of the solution so as to transform the CO<sub>2</sub> into CO<sub>3</sub><sup>2-</sup> or HCO<sub>3</sub><sup>-</sup>. These latter species, however, are more stable and more difficult to be reduced than CO<sub>2</sub> itself. The competitive development of H<sub>2</sub> can be observed because the activation of H<sub>2</sub>O is much simpler than that of CO<sub>2</sub> and the redox potential of H<sub>2</sub>O into H<sub>2</sub> is close to that of CO<sub>2</sub> reduction. Also, while electrons reduce CO<sub>2</sub>, a sacrificial hole trap is needed. Water, in addition to behaving like a solvent, can work as a sacrificial molecule. In many cases, however, sacrificial electron donors such as 2-propanol<sup>[138,145]</sup> and triethanolamine are used to overcome the kinetic and thermodynamic drawbacks linked to the oxidation reaction.<sup>[27]</sup> Nevertheless, the selectivity towards the products can be overestimated because C<sub>1</sub> hydrocarbons can be formed by oxidation of sacrificial species.

A further important problem in the use of water as a solvent is due to the solubility in it of most CO<sub>2</sub> reduction products, making their recovery difficult. Some of these weaknesses can be overcome by carrying out the reaction in the gas phase. Xie et al.<sup>[167]</sup> compared the activity of various TiO<sub>2</sub> samples in liquid-solid and gas-solid systems and reported that the selectivity was higher in gas phase where no H<sub>2</sub> evolution was observed. The rates of formation of CO and CH<sub>4</sub> in the gas-solid reactor were higher than in the liquid-solid one.

Another important issue is the presence of organic residues on the catalyst surface which can give rise to products under irradiation. It has been demonstrated by *in situ* DRIFT spectroscopy in the presence of isotopically labelled <sup>13</sup>CO<sub>2</sub> that, during CO<sub>2</sub> reduction, along with small amounts of <sup>13</sup>CO, <sup>12</sup>CO deriving from carbon impurities present on the catalyst surface can be formed as the main product.<sup>[177]</sup> Impurities are due either to organic molecules present in the environment to which the catalyst is exposed or to organic precursors that are often used during the synthesis process. To be sure that the detected products derive from CO<sub>2</sub> reduction rather than carbonaceous

residues, it is advisable to choose inorganic precursors and clean the surface of the catalysts very carefully before their use. The procedure reported by Mei et al., for instance, is recommended.<sup>[178]</sup> Moreover, it is useful to carry out some tests using labelled <sup>13</sup>CO<sub>2</sub> to check that the products derive from the reduction of carbon dioxide. Runs in the presence of water vapour but in the absence of CO<sub>2</sub>, resulted in CH<sub>4</sub> formation from carbon residues that were present on the catalyst surface.<sup>[163]</sup> However, its quantity was very low and in any case negligible compared to the CH<sub>4</sub> formed by CO<sub>2</sub> reduction (Figure 12).

## 4. Photoelectrocatalysis

Photoelectrocatalysis combines photocatalysis and electrocatalysis trying to overcome the limits of the single technologies. The process set-up is similar to that used in electrocatalysis, the difference relies in the replacement of a normal conducting electrode with an irradiated semiconductor electrode (Figure 13). Sometimes semiconductors are used both as photocathode and as photoanode. Briefly, the photoelectrode harvests the incident photons generating the e<sup>-</sup>/h<sup>+</sup> pair, and the band bending that occurs at the semiconductor-electrolyte interface gives rise to an electric field inside the semiconductor which separates the electron-hole pairs. Moreover, the application of an external potential can further improve charge separation. Electrons reduce CO<sub>2</sub> at the photoelectrode-electrolyte interface while the holes migrate to the counter electrode and accumulate at the electrocatalyst-electrolyte interface where they take part in the oxidation process. A more detailed description of the various cell types is given elsewhere.<sup>[206,207]</sup>

The photoelectrocatalytic (PEC) method represents a valid alternative for CO<sub>2</sub> reduction and it presents some advantages with respect to the simple electrocatalytic method and to heterogeneous photocatalysis. Firstly, it is possible to reduce electricity consumption as the use of an external power source such as solar energy or solar panels allows to reduce the applied voltage. Second, the efficiency of the process is generally higher, as the application of an external bias allows for better separation of the photogenerated charges. It should also be noted that the use of two separate cells avoids the oxidation of organic substances produced such as methanol, which is oxidized by the holes more easily than H<sub>2</sub>O. By varying the experimental conditions, and in particular the type of photoelectrodes used, it is possible to obtain a variety of products with different yields.

The photoelectrocatalytic reduction of CO<sub>2</sub> was carried out for the first time in 1978 by Halmann.<sup>[208]</sup> The reaction was carried out in an aqueous solution of carbon dioxide and a *p*-type GaP semiconductor was used as a photocathode. The products obtained were HCOOH, HCHO and CH<sub>3</sub>OH. Numerous studies have been conducted since then. Table 4 shows some of the photoelectrocatalytic systems used for CO<sub>2</sub> reduction.

The analysis of Table 4 shows that generally Pt-based electrodes are used as anode while materials of various types have been tested in the cathode compartment. The most used



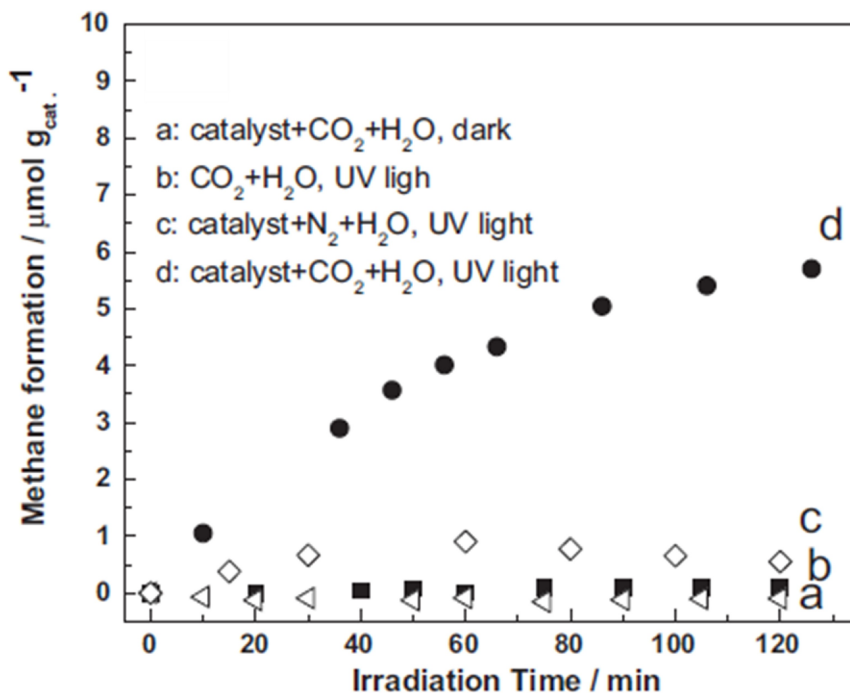


Figure 12. Methane formation versus irradiation time in the presence of 0.2 Pt/TiO<sub>2</sub> sample under different conditions. Reproduced with permission from Ref. [163] Copyright (2012) Elsevier.

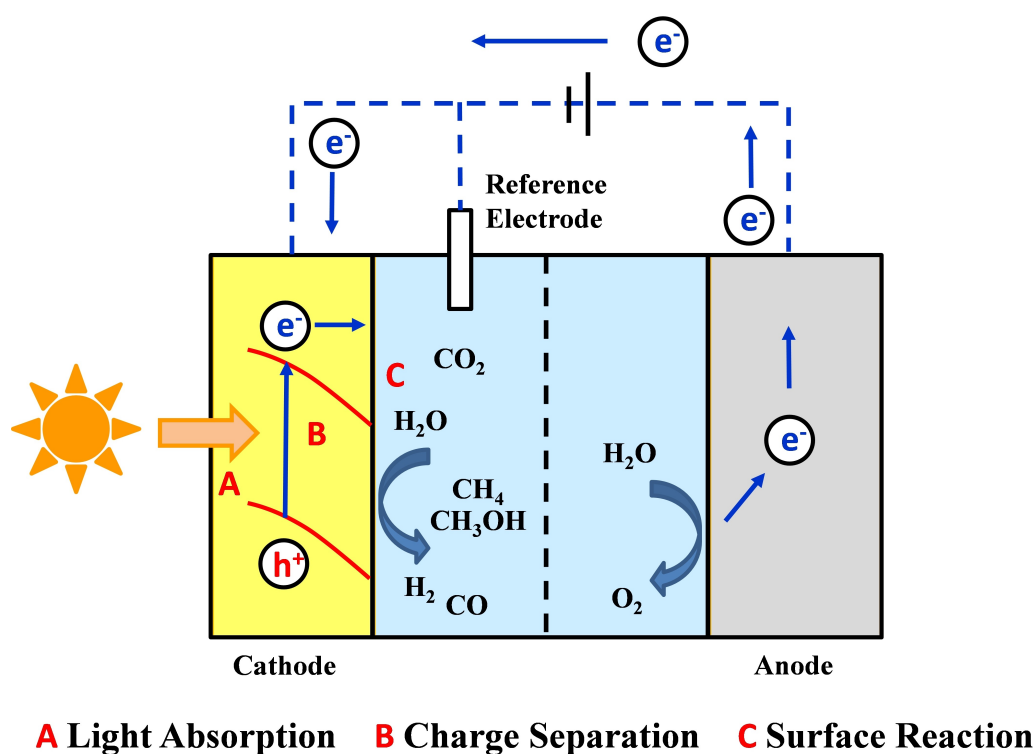


Figure 13. Scheme of a photoelectrochemical cell for CO<sub>2</sub> reduction and water oxidation.

ones are semiconductors active under the irradiation of visible light to minimize energy costs. A greater variety of products is obtained compared to the photocatalytic method and faradic efficiencies are generally higher. The mechanism of formation

of CO<sub>2</sub> reduction products is similar to that found during photocatalytic tests, especially when the same materials are used.

Table 4. Some representative photoelectrocatalytic systems for CO<sub>2</sub> reduction.

Electrode	Electrolyte	Light source and time	Selectivity (Products)	Faradaic Efficiency [%]	Potential [V]	Ref.
Photocathode: p-GaP Anode: carbon rod	K <sub>2</sub> HPO <sub>4</sub> /KH <sub>2</sub> PO <sub>4</sub>	Hg lamp, 90 h	HCOOH 50 mM HCHO 0.28 mM CH <sub>3</sub> OH 0.81 mM HCOOH 0.17 mM	–	–1.0 V vs. SCE	[208]
Photocathode: Ru complex modified Zn-doped p-InP Anode: glassy carbon	H <sub>2</sub> O	Visible light, 3 h	HCOOH 0.49 mM	62%	–0.6 V vs. Ag/AgCl	[209]
Photocathode: Ru complex polymer modified Cu <sub>2</sub> ZnSnS <sub>4</sub> Anode: glassy carbon	H <sub>2</sub> O	Visible light, 3 h	HCOOH 0.49 mM	80%	–0.4 V vs. Ag/AgCl	[210]
Anode: glassy carbon Photocathode: p-Si + Re(bipy-tBu)(CO) <sub>3</sub> Cl	CH <sub>3</sub> CN/H <sub>2</sub> O	661 nm, 2.5 h	H <sub>2</sub> + CO (H <sub>2</sub> /CO = 2:1) j = 5.6 mA cm <sup>-2</sup>	100%	–1.9 V vs. Fc/Fc <sup>+</sup>	[211]
Anode: Pt electrode Photocathode: Re(bipy-tBu)(CO) <sub>3</sub> Cl + TiO <sub>2</sub> -protected Cu <sub>2</sub> O	CH <sub>3</sub> OH	AM 1.5, 5.5 h	CO (j = 1.5 mA cm <sup>-2</sup> )	100%	–1.73 V vs. Fc/Fc <sup>+</sup>	[212]
Anode: Pt electrode Photocathode: Re complex + zinc porphyrin + p-type NiO	Bu <sub>4</sub> NBF <sub>4</sub> in DMF	430 nm	CO 0.93 μmol	6.2%		[213]
Anode: Pt electrode Photocathode: Ru(II)-Re(I)/p-NiO	Et <sub>4</sub> NBF <sub>4</sub> in DMF-TEA, Ag/AgNO <sub>3</sub>	λ > 460 nm, 5 h	CO 255 nmol	98%	–1.2 V vs. Ag/AgCl	[214]
Anode: Pt electrode Photocathode: polypyrrole-coated p-ZnTe	KHCO <sub>3</sub>	λ > 420 nm, 6 h	HCOOH 131 nmol h <sup>-1</sup> cm <sup>-2</sup> CO 50 nmol h <sup>-1</sup> cm <sup>-2</sup> H <sub>2</sub> 108 nmol h <sup>-1</sup> cm <sup>-2</sup> CO 68 μmol cm <sup>-2</sup>		–0.3 V vs. SCE	[215]
Anode: carbon rod	KHCO <sub>3</sub>	λ > 420 nm, 1 h		CO 23% H <sub>2</sub> 61%	–0.7 V vs. RHE	[216]
Photocathode: ZnTe/ZnO nanowire/Zn substrate Anode: Pt electrode	Na <sub>2</sub> SO <sub>4</sub> (pH 10)	AM 1.5, 10 h	HCOOH + CO + H <sub>2</sub> , j = 1 mA cm <sup>-2</sup>		0.25 V vs. RHE	[217]
Photocathode: CuO nanowires/p-Cu <sub>2</sub> O/Cu Anode: Pt electrode	KHCO <sub>3</sub>	visible light, 1 h	CH <sub>3</sub> OH 0.1 μmol h <sup>-1</sup> cm <sup>-2</sup> HCOOH 0.52 μmol h <sup>-1</sup> cm <sup>-2</sup> CO 0.24 μmol h <sup>-1</sup> cm <sup>-2</sup>		–0.4 V vs. SCE	[218]
Photocathode: Pb/CuO/Cu <sub>2</sub> O film Anode: carbon rod	Na <sub>2</sub> CO <sub>3</sub> /NaHCO <sub>3</sub>	UV-vis light, 2 h	CH <sub>3</sub> OH: 82 ppm HCHO: 50.6 ppm HCOOH 6.8 mmol L <sup>-1</sup> cm <sup>-2</sup>	100%	0.2 V vs. Ag/AgCl	[219]
Photocathode: Cu/Cu <sub>2</sub> O electrode Anode: Pt electrode	Na <sub>2</sub> SO <sub>4</sub>	UV-vis light, 8 h			–0.9 V vs. SCE	[220]
Co <sub>3</sub> O <sub>4</sub> nanotube arrays Anode: Pt electrode	KHCO <sub>3</sub>	AM 1.5, 24 h	HCOOH 5 μmol h <sup>-1</sup>	Solar to chemical energy efficiency: 1%	no external bias potential	[221]
Photocathode: CuFeO <sub>2</sub> /CuO Anode: Pt electrode	NaHCO <sub>3</sub>	470 nm, 15 h	HCOO <sup>-</sup> H <sub>2</sub>	Solar to chemical energy efficiency: 14%	–0.9 V vs. SCE	[222]
Photocathode: Ti/ZnO-Fe <sub>2</sub> O <sub>3</sub> Anode: Pt electrode	KHCO <sub>3</sub>	λ > 420 nm, 6 h	CH <sub>3</sub> OH 14.5 mmol L <sup>-1</sup>	100% Solar to chemical energy efficiency: 0.45%	–1.3 V vs. SCE	[223]
Photocathode: MoS <sub>2</sub> -rods/TiO <sub>2</sub> NTs Anode: Pt electrode	NaHCO <sub>3</sub>	300 W xenon lamp (400 nm < λ < 800 nm, 3 h) UV light, 1.5 h	CH <sub>3</sub> OH 0.773 mmol cm <sup>-2</sup> CH <sub>3</sub> OH 0.88 mmol L <sup>-1</sup> C <sub>2</sub> H <sub>5</sub> OH 2.60 mmol L <sup>-1</sup> CH <sub>3</sub> COCH <sub>3</sub> 0.049 mmol L <sup>-1</sup>	96.5%	0.5 V vs. RHE	[224]
Photocathode: Si/TiO <sub>2</sub> /Pt Anode: Pt electrode					0.5 V vs. RHE	[225]

Electrode	Electrolyte	Light source and time	Selectivity (Products)	Faradaic Efficiency [%]	Potential [V]	Ref.
<i>Cathode:</i> Pt- RGO <i>Photoanode:</i> Pt/TiO <sub>2</sub> nanotubes	NaCl + NaHCO <sub>3</sub>	Xe arc lamp, 8 h	HCOOH + CH <sub>3</sub> OH + CH <sub>3</sub> COOH + C <sub>2</sub> H <sub>5</sub> OH 1.5 μmol h <sup>-1</sup> cm <sup>-2</sup>	81 %	2 V vs. RHE	[226]
<i>Cathode:</i> Ti/TiO <sub>2</sub> NT-ZrO <sub>2</sub> <i>Photoanode:</i> DSA	Na <sub>2</sub> SO <sub>4</sub>	UV light, 2 h	CH <sub>3</sub> OH 485 μmol L <sup>-1</sup> C <sub>2</sub> H <sub>5</sub> OH 268 μmol L <sup>-1</sup> CH <sub>4</sub> : 0.7 μmol cm <sup>-2</sup>	67 %	-0.3 V vs. Ag/AgCl	[227]
<i>Cathode:</i> Cu <i>Photoanode:</i> WO <sub>3</sub>	KHCO <sub>3</sub>	λ > 420 nm, 1 h			0.75 V vs. RHE	[228]
<i>Photocathode:</i> p-InP/hybrid Ru complex polymer <i>Photoanode:</i> Pt/TiO <sub>2</sub>	NaHCO <sub>3</sub>	AM 1.5, 24 h	HCOOH 5.2 μmol cm <sup>-2</sup>	Solar to chemical energy efficiency: 0.03 %	no applied bias	[229]
<i>Photocathode:</i> InP/hybrid Ru complex polymer <i>Photoanode:</i> reduced SrTiO <sub>3</sub>	NaHCO <sub>3</sub>	Photocathode λ > 420 nm, photoanode AM 1.5, 3 h	HCOOH 1.5 μmol	Solar to chemical energy efficiency: 0.14 %	no applied bias	[230]

A very promising oxide could be Cu<sub>2</sub>O given the good results obtained when used as a photocathode in the photoelectrochemical reduction of water.<sup>[231]</sup> However, Cu<sub>2</sub>O is unstable under irradiation as Cu<sup>+</sup> can be reduced to Cu<sup>0</sup>. A strategy to avoid this drawback is coupling Cu<sub>2</sub>O with other oxides, the addition of other species and heat treatment that give rise to the formation of heterostructures.<sup>[217,221,232,233]</sup>

De Brito et al.<sup>[219]</sup> performed the photoelectrochemical reduction under visible light irradiation of CO<sub>2</sub> by using a Cu/Cu<sub>2</sub>O electrode as photocathode. They observed the formation of methanol, ethanol, formaldehyde, acetaldehyde, and acetone in different amounts by varying the applied potential (Figure 14). The highest percentage of reduced CO<sub>2</sub> and the highest amount of methanol were obtained at 0.2 V. The amount of each product varied with the electrolysis time, methanol was detected in the first 30 minutes while acetaldehyde and acetone for times longer than 120 minutes. Also in this case the role of the Cu<sup>2+</sup>/Cu<sup>+</sup> redox couple in the reduction process was highlighted.

Cu<sub>2</sub>O/CuO nanowires grown on a Cu foil as substrate were effective for the photoelectrocatalytic CO<sub>2</sub> reduction in aqueous solutions under solar light irradiation, forming CO, HCOOH, and H<sub>2</sub>.<sup>[217]</sup>

Pb/CuO/Cu<sub>2</sub>O film exhibited a significant performance reaching a faradaic efficiency of about 40 % at -0.16 V (vs. SHE) under visible light irradiation in aqueous solution.<sup>[233]</sup> Formic acid (0.524 μmol h<sup>-1</sup> cm<sup>-2</sup>) and methanol (0.102 μmol h<sup>-1</sup> cm<sup>-2</sup>) were the main products.

Co<sub>3</sub>O<sub>4</sub> is a good photocatalyst from the point of view of the possible use under sunlight, due to its band-gap (about 2 eV). However, it showed low activity towards CO<sub>2</sub> reduction due to the high recombination rate of the e<sup>-</sup>/h<sup>+</sup> pairs. The addition of a different species, however, showed beneficial effects on the activity.

By using Cu/Co<sub>3</sub>O<sub>4</sub> metal nanotubes as cathode, formate was obtained as the main product (6.8 mmol L<sup>-1</sup> cm<sup>-2</sup> in 8 h) with a selectivity of almost 100%.<sup>[220]</sup> The formation rate of formate was 56 % greater than that obtained in the presence of bare Co<sub>3</sub>O<sub>4</sub>. Formate formation was explained by considering a two-electron reduction mechanism. The transfer of the first electron led to the formation of the CO<sub>2</sub><sup>•-</sup> radical adsorbed on Cu. Successively, the transfer of a proton forms the radical HCOO<sup>•</sup> which desorbs from the Cu surface by transferring an electron to the adsorbed species.

The quantity and type of products formed can be varied by coupling a photoanode with different cathode materials. Magesh et al.<sup>[228]</sup> compared the efficiency during CO<sub>2</sub> reduction under visible light irradiation in two cells containing WO<sub>3</sub> as the photoanode and Cu or Sn/SnO<sub>x</sub> as the cathode (Figure 15). CH<sub>4</sub> (with a faradaic efficiency of 67 %) and H<sub>2</sub> were the main products using Cu, while HCOOH and CO (with a CO + HCOOH faradic efficiency of 44 %) with Sn/SnO<sub>x</sub>.

The application of an external bias is usually required to perform CO<sub>2</sub> reduction. Nevertheless, Kang et al.<sup>[221]</sup> demonstrated recently that CuFeO<sub>2</sub>/CuO binary films used as photocathodes were effective in the photoelectrocatalytic reduction of CO<sub>2</sub> to formate without the application of external bias. The

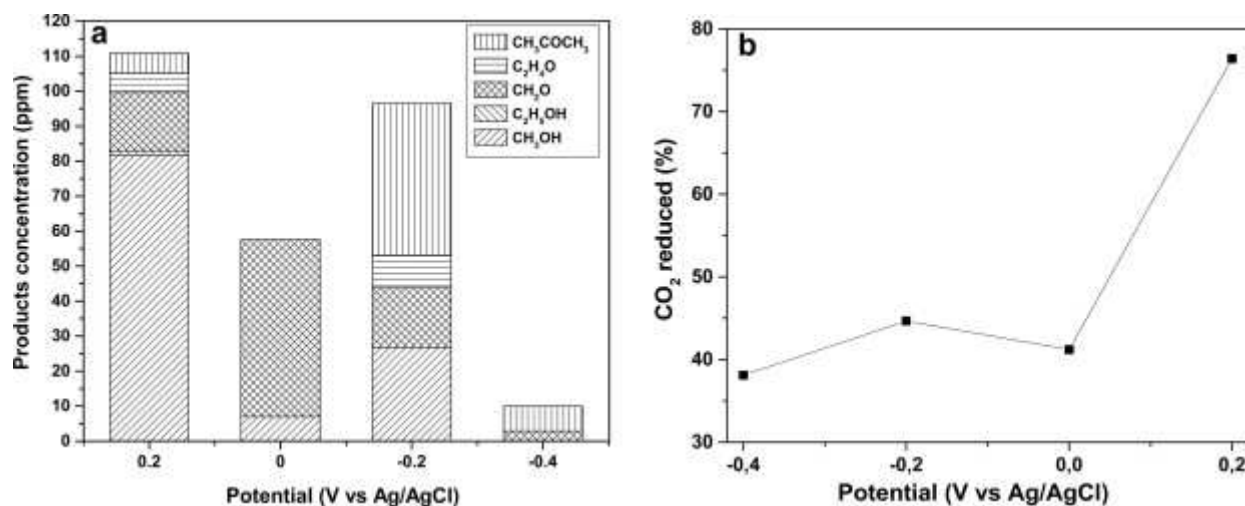


Figure 14. (a) Amount of products formed after 2 h of irradiation and (b) percentage of CO<sub>2</sub> reduced at different potential values. Reproduced with permission from Ref. [219] Copyright (2015) Elsevier.

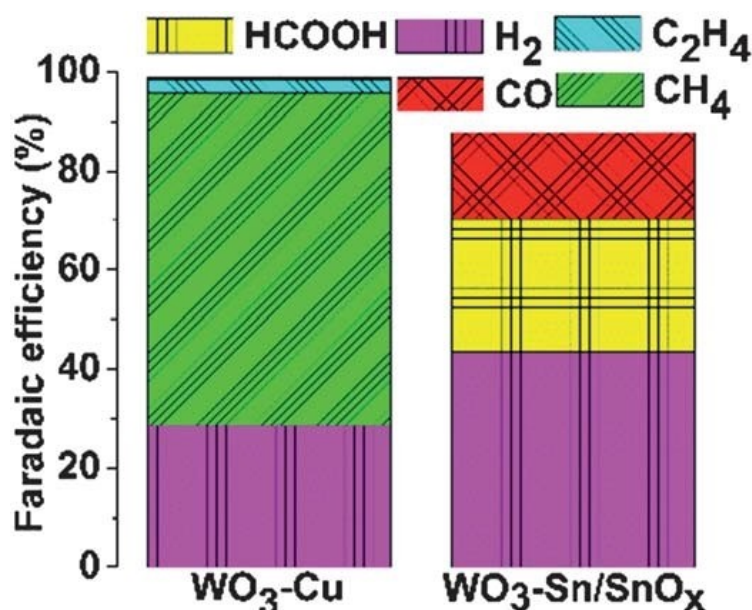
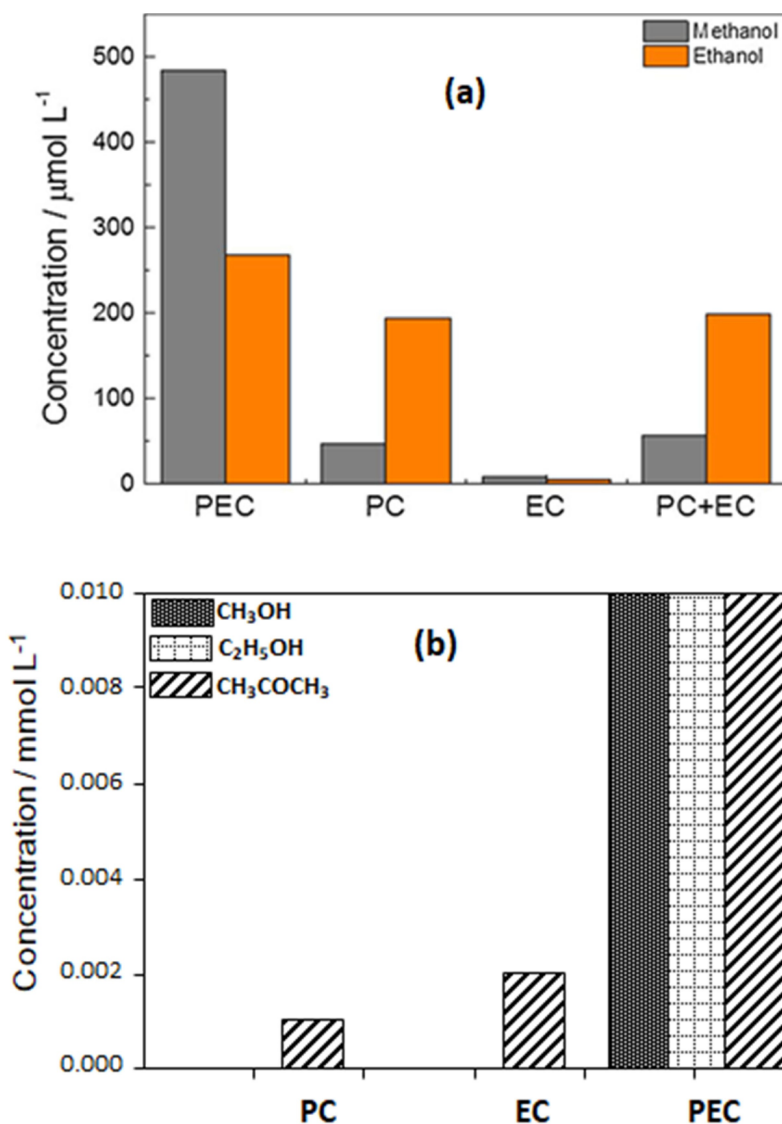


Figure 15. Distribution of the CO<sub>2</sub> reduction products by using different anodic materials. Reproduced with permission from Ref. [228] Copyright (2014) Royal Society of Chemistry.

reaction was carried out under simulated sunlight irradiation with a selectivity towards formate greater than 90% at 0.9 V vs. RHE and a solar to formate energy conversion efficiency of approximately 1%. O<sub>2</sub> was formed from water in the anode compartment. Furthermore, formate production continued for 1 week reaching 250 μmol with a small decrease in cell potential from 230 mV to 170 mV.

Lima Perini et al.<sup>[227]</sup> compared the efficiency towards CO<sub>2</sub> reduction in photocatalysis, electrocatalysis and photoelectrocatalysis using Ti/TiO<sub>2</sub> nanotubes-ZrO<sub>2</sub> as cathode dipped in a Na<sub>2</sub>SO<sub>4</sub> solution under UV irradiation and applying a potential of -0.3 V (Figure 16 a). Negligible quantities of ethanol (4.7 μmolL<sup>-1</sup>) and methanol (9.2 μmolL<sup>-1</sup>) were obtained by electrocatalysis, while larger quantities (194 and 47 μmolL<sup>-1</sup>,

respectively) were formed using the photocatalytic method. With a combined approach, larger quantities of ethanol (268 μmolL<sup>-1</sup>) and methanol (485 μmolL<sup>-1</sup>) were formed than those of the single approaches, confirming a synergistic effect between photocatalysis and electrocatalysis. Similar results have been reported by other investigators.<sup>[225,234–236]</sup> In particular, by using a highly porous Si/TiO<sub>2</sub>/Pt p-n junction as the semiconductor for CO<sub>2</sub> reduction in a saturated solution, a good photocurrent response (-1.0 mA under -0.8 V) was observed in the cathodic compartment under UV-vis irradiation.<sup>[225]</sup> Methanol, ethanol and acetone were the main observed compounds, and also in this case the highest amounts were obtained by the combined photoelectrocatalytic approach (Figure 16 b)



**Figure 16.** Evaluation of  $\text{CO}_2$  reduction products formed after 1 h using photoelectrocatalysis (PEC), photocatalysis (PC), and electrocatalysis (EC). (a)  $\text{Ti/TiO}_2\text{-ZrO}_2$ , (b)  $\text{Si/TiO}_2/\text{Pt}$ . Reproduced with permission from Refs. [227] and [225] for (a) and (b), respectively. Copyright (2018) and (2015) Elsevier.

Formate was selectively formed under visible light irradiation in the presence of hierarchical structured  $\text{Co}_3\text{O}_4$  electrode.<sup>[234]</sup> The synergy between photocatalysis and electrocatalysis (Figure 17) allowed to obtain a very high formate production reaching ca.  $385 \mu\text{mol}$  within 8 h.

The efficiency of  $\text{CO}_2$  reduction in a PEC system can be low, in many cases, because the preferential reduction of water could compete at the surface of p-type semiconductors. In this case, by applying a large bias, it is possible to shift the valence band of the semiconductor to less positive values, hindering the undesired reaction. However, the instability due to irradiation of the materials that make up the electrodes must be considered, which often induces photocorrosion phenomena and this is one of the main drawbacks of the photoelectrochemical method. To use sunlight, semiconductors with a low band gap are often used, but they can be inert for the activation of  $\text{CO}_2$ , therefore it is necessary to add co-catalysts

capable of activating the  $\text{CO}_2$  molecule and enhancing the charge transfer process.

## 5. Conclusions and Perspectives

Given the environmental problems, the capture and use of  $\text{CO}_2$  is one of the most significant and challenging field of research. Different approaches are possible and the electrochemical and photocatalytic methods can be cited as the most promising, although they display some feebleness that can be overcome by taking a cue from the results obtained so far. The efficiency of the electrocatalytic process could be improved by exploring the use of multi-catalyst electrodes to exploit the properties of the different functionalities and avoid the use of noble metal particles.

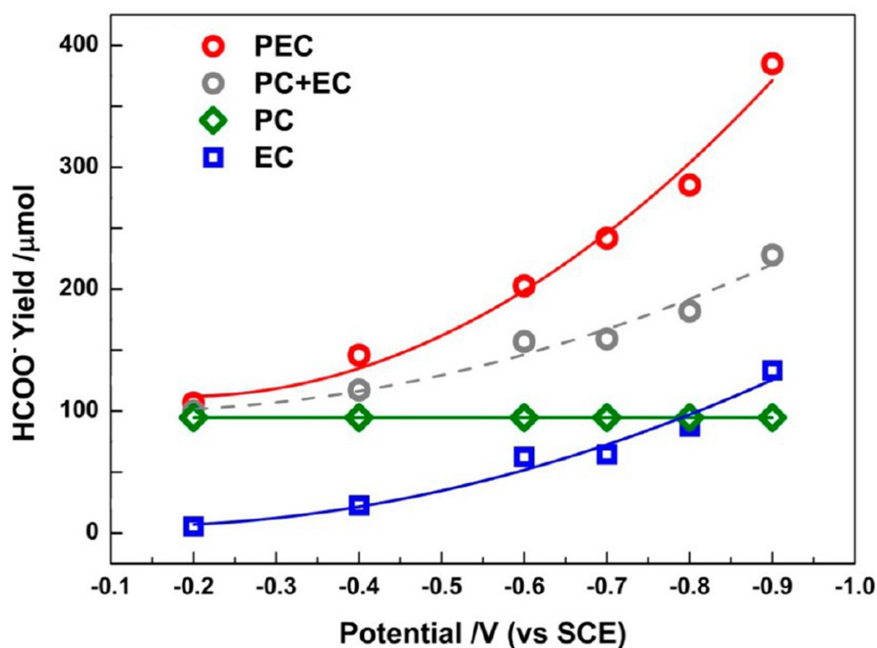


**Figure 17.** Formate yields under PC, EC and PEC conditions by applying different negative potentials. Reproduced with permission from Ref. [234] Copyright (2013) American Chemical Society.

This strategy could be useful also in the photocatalytic approach by coupling solar light responsive semiconductors with one or more (photo)catalyst bearing basic and adsorbent surface sites.

The photoelectrocatalytic method can mitigate/overcome the weaknesses of both photocatalysis and electrocatalysis and minimize the simultaneous formation of H<sub>2</sub>. In fact, it allows to increase the efficiency of CO<sub>2</sub> reduction and direct the selectivity towards certain products. The appropriate choice of the semiconductors and of some process parameters, such as the applied potential, is required to achieve optimised performances. However, it should be noted that sometimes one of the three methods can be more successful than the others, depending on the operating conditions and on the desired product(s).

Despite the progress realized over the last few years, the PEC process still presents hurdles to be faced such as the low solubility of CO<sub>2</sub> in water at ambient conditions, the high applied potential, the formation of a mixture of compounds which must then be separated, and the progressive deactivation and possible photocorrosion of the photoelectrodes.

To overcome these drawbacks, an effort is needed (i) to develop catalysts that exhibit high activity towards CO<sub>2</sub> reduction under sunlight irradiation, (ii) to design active sites on the surface of catalysts that allow good CO<sub>2</sub> adsorption, (iii) to prepare highly selective and stable catalysts, (iv) to optimize the experimental conditions of the reaction in order to obtain high efficiency with low energy costs, (v) to deepen the knowledge of the reaction mechanism in different experimental conditions, (vi) to scale-up the process for practical applications.

## Acknowledgements

Open Access Funding provided by Politecnico di Milano within the CRUI-CARE Agreement.

## Conflict of Interest

The authors declare no conflict of interest.

**Keywords:** carbon dioxide reduction · electrocatalysis · photocatalysis · photo-electrocatalysis

- [1] S. N. Habisreutinger, L. Schmidt-Mende, J. K. Stolarczyk, *Angew. Chem. Int. Ed.* **2013**, *52*, 7372–7408; *Angew. Chem.* **2013**, *125*, 7516–7557.
- [2] G. Centi, S. Perathoner, *Catal. Today* **2009**, *148*, 191–205.
- [3] S. Wang, X. Han, Y. Zhang, N. Tian, T. Ma, H. Huang, *Small Structures* **2021**, *2*, 2000061.
- [4] N. Mulchandani, V. Katiyar (2020) Polymers from Carbon Dioxide – A Route Towards a Sustainable Future. In: Katiyar V., Kumar A., Mulchandani N. (eds) *Advances in Sustainable Polymers. Materials Horizons: From Nature to Nanomaterials*. Springer, Singapore.
- [5] Y. Qin, X. Wang (2019) Conversion of CO<sub>2</sub> into Polymers. In: Han B., Wu T. (eds) *Green Chemistry and Chemical Engineering. Encyclopedia of Sustainability Science and Technology Series*. Springer, New York, NY.
- [6] M. Aresta, A. Dibenedetto, *J. Mol. Catal. A* **2002**, *182–183*, 399–409.
- [7] S. Sato, T. Arai, T. Morikawa, K. Uemura, T. M. Suzuki, H. Tanaka, T. Kajino, *J. Am. Chem. Soc.* **2011**, *133*, 15240–15243.
- [8] G. A. Olah, A. Goepfert, G. K. Surya Prakash, *J. Org. Chem.* **2009**, *74*, 487–498.
- [9] A. A. Olajire, *J. CO<sub>2</sub> Util.* **2013**, *3–4*, 74–92.
- [10] H. Yang, C. Zhang, P. Gao, H. Wang, X. Li, L. Zhong, W. Wei, Y. Sun, *Catal. Sci. Technol.* **2017**, *7*, 4580–4598.
- [11] S. C. Roy, O. K. Varghese, M. Paulose, C. A. Grimes, *ACS Nano* **2010**, *4*, 1259–1278.
- [12] W. Tu, Y. Zhou, Z. Zou, *Adv. Mater.* **2014**, *26*, 4607–4626.

- [13] X. Chang, T. Wang, J. Gong, *Energy Environ. Sci.* **2016**, *9*, 2177–2196.
- [14] T. P. Nguyen, D. L. T. Nguyen, V.-H. Nguyen, T.-H. Le, D.-V. N. Vo, Q. T. Trinh, S.-R. Bae, S. Y. Chae, S. Y. Kim, Q. V. Le, *Nanomaterials* **2020**, *10*, 337.
- [15] R. Kortlever, J. Shen, K. J. P. Schouten, F. Calle-Vallejo, M. T. M. Koper, *J. Phys. Chem. Lett.* **2015**, *6*, 4073–4082.
- [16] J. Wu, T. Sharifi, Y. Gao, T. Zhang, P. M. Ajayan, *Adv. Mater.* **2019**, *31*, 1804257.
- [17] E. E. Benson, C. P. Kubiak, A. J. Sathrum, J. M. Smieja, *Chem. Soc. Rev.* **2009**, *38*, 89–99.
- [18] V. Kumaravel, J. Bartlett, S. C. Pillai, *ACS Energy Lett.* **2020**, *5*, 486–519.
- [19] M. Aresta, A. Dibenedetto, C. Pastore, *Environ. Chem. Lett.* **2005**, *3*, 113–117.
- [20] J.-H. Jeoung, H. Dobbek, *Science* **2007**, *318*, 1461–1464.
- [21] Y. Wang, D. He, H. Chen, D. i Wang, *J. Photochem. Photobiol.* **2019**, *40*, 117–149.
- [22] T. Kong, Y. Jiang, Y. Xiong, *Chem. Soc. Rev.* **2020**, *49*, 6579–6591.
- [23] Y. Bo, C. Gao, Y. Xiong, *Nanoscale* **2020**, *12*, 12196–12209.
- [24] F. Parrino, M. Bellardita, E. I. García-López, G. Marci, V. Loddò, L. Palmisano, *ACS Catal.* **2018**, *8*, 11191–11225.
- [25] S. Liang, N. Altaf, L. Huang, Y. Gao, Q. Wang, *J. CO<sub>2</sub> Util.* **2020**, *35*, 90–105.
- [26] J. Yuan, Y. Du, H. Zhang, *APL Mater.* **2020**, *8*, 060904.
- [27] J. He, C. Janáky, *ACS Energy Lett.* **2020**, *5*, 1996–2014.
- [28] D. T. Whipple, P. J. A. Kenis, *J. Phys. Chem. Lett.* **2010**, *1*, 3451–3458.
- [29] J. Wang, Y. Guan, X. Yu, Y. Cao, J. Chen, Y. Wang, B. Hu, H. Jing, *iScience* **2020**, *23*, 100768.
- [30] T. Burdyny, W. A. Smith, *Energy Environ. Sci.* **2019**, *12*, 1442–1453.
- [31] E. V. Kondratenko, G. Mul, J. Baltrusaitis, G. O. Larrázabal, J. Pérez-Ramírez, *Energy Environ. Sci.* **2013**, *6*, 3112–3135.
- [32] C. Costentin, M. Robert, J.-M. Savéant, *Chem. Soc. Rev.* **2013**, *42*, 2423–2436.
- [33] K. Tanaka, D. Ooyama, *Coord. Chem. Rev.* **2002**, *226*, 211–218.
- [34] Y. Hori, H. Wakebe, T. Tsukamoto, O. Koga, *Electrochim. Acta* **1994**, *39*, 1833–1839.
- [35] D. L. T. Nguyen, M. S. Jee, D. H. Won, H. Jung, H.-S. Oh, B. K. Min, Y. J. Hwang, *ACS Sustainable Chem. Eng.* **2017**, *5*, 11377–11386.
- [36] D. L. T. Nguyen, M. S. Jee, D. H. Won, H. Jung, H.-S. Oh, B. K. Min, Y. J. Hwang, *Catal. Commun.* **2018**, *114*, 109–113.
- [37] X. Jiang, F. Cai, D. Gao, J. Dong, S. Miao, G. Wang, X. Bao, *Electrochem. Commun.* **2016**, *68*, 67–70.
- [38] T. Zhang, X. Li, Y. Qiu, P. Su, W. Xu, H. Zhong, H. Zhang, *J. Catal.* **2018**, *357*, 154–162.
- [39] F. Quan, D. Zhong, H. Song, F. Jia, L. Zhang, *J. Mater. Chem. A* **2015**, *3*, 16409–16413.
- [40] W. Luo, J. Zhang, M. Li, A. Züttel, *ACS Catal.* **2019**, *9*, 3783–3791.
- [41] X. Jiang, F. Cai, D. Gao, J. Dong, S. Miao, G. Wang, X. Bao, *Electrochem. Commun.* **2016**, *68*, 67–70.
- [42] H. Won da, H. Shin, J. Koh, J. Chung, H. S. Lee, H. Kim, S. I. Woo, *Angew. Chem. Int. Ed.* **2016**, *55*, 9297–9300; *Angew. Chem.* **2016**, *128*, 9443–9446.
- [43] Y. Lu, B. Han, C. Tian, J. Wu, D. Geng, D. Wang, *Electrochem. Commun.* **2018**, *97*, 87–90.
- [44] V. S. K. Yadav, M. K. Purkait, *New J. Chem.* **2015**, *39*, 7348–7354.
- [45] T. Zhang, H. Zhong, Y. Qiu, X. Li, H. Zhang, *J. Mater. Chem. A* **2016**, *4*, 16670–16676.
- [46] Y. Hori, K. Kikuchi, S. Suzuki, *Chem. Lett.* **1985**, *14*, 1695–1698.
- [47] K. W. Frese, *J. Electrochem. Soc.* **1991**, *138*, 3338–3344.
- [48] M. Schwartz, R. L. Cook, V. M. Kehoe, R. C. Macduff, J. Patel, A. F. Sammells, *J. Electrochem. Soc.* **1993**, *140*, 614–618.
- [49] Y. Lan, S. Ma, J. Lu, P. J. A. Kenis, *Int. J. Electrochem. Sci.* **2014**, *9*, 7300–7308.
- [50] M. Le, M. Ren, Z. Zhang, P. T. Sprunger, R. L. Kurtz, J. C. Flake, *J. Electrochem. Soc.* **2011**, *158*, E45–E49.
- [51] M. Gattrell, N. Gupta, A. Co, *J. Electroanal. Chem.* **2006**, *594*, 1–19.
- [52] K. Gupta, M. Bersani, J. A. Darr, *J. Mater. Chem. A* **2016**, *4*, 13786–13794.
- [53] F. S. Roberts, K. P. Kuhl, A. Nilsson, *Angew. Chem. Int. Ed.* **2015**, *54*, 5179–5182; *Angew. Chem.* **2015**, *127*, 5268–5271.
- [54] K. D. Yang, W. R. Ko, J. H. Lee, S. J. Kim, H. Lee, M. H. Lee, K. T. Nam, *Angew. Chem. Int. Ed.* **2017**, *56*, 796–800; *Angew. Chem.* **2017**, *129*, 814–818.
- [55] K. Manthiram, B. J. Beberwyck, A. P. Alivisatos, *J. Am. Chem. Soc.* **2014**, *136*, 13319.
- [56] H. Mistry, A. S. Varela, C. S. Bonifacio, I. Zegkinoglou, I. Sinev, Y.-W. Choi, K. Kisslinger, E. A. Stach, J. C. Yang, P. Strasser, B. R. Cuenya, *Nat. Commun.* **2016**, *7*, 12123.
- [57] A. H. Shah, Y. Wang, A. R. Woldu, L. Lin, M. Iqbal, D. Cahen, *J. Phys. Chem. C* **2018**, *122*, 18528–18536.
- [58] Y. Hori, I. Takahashi, O. Koga, N. Hoshi, *J. Mol. Catal. A* **2003**, *199*, 39–47.
- [59] K. J. P. Schouten, E. Pérez Gallent, M. T. Koper, *ACS Catal.* **2013**, *3*, 1292–1295.
- [60] W. Zhu, R. Michalsky, O. Metin, H. Lv, S. Guo, C. J. Wright, X. Sun, A. A. Peterson, S. Sun, *J. Am. Chem. Soc.* **2013**, *135*, 16833–16886.
- [61] H. Mistry, R. Reske, Z. Zeng, Z. J. Zhao, J. Greeley, P. Strasser, B. R. Cuenya, *J. Am. Chem. Soc.* **2014**, *136*, 16473–16476.
- [62] W. Zhu, Y. J. Zhang, H. Zhang, H. Lv, Q. Li, R. Michalsky, A. A. Peterson, S. Sun, *J. Am. Chem. Soc.* **2014**, *136*, 16132–16135.
- [63] N. Hoshi, M. Kato, Y. Hori, *J. Electroanal. Chem.* **1997**, *440*, 283–286.
- [64] T. Hatsukade, K. P. Kuhl, E. R. Cave, D. N. Abram, T. F. Jaramillo, *Phys. Chem. Chem. Phys.* **2014**, *16*, 13814–13819.
- [65] A. V. Rudnev, K. Kiran, A. Cedeño López, A. Dutta, I. Gjuroski, J. Furrer, P. Broekmann, *Electrochim. Acta* **2019**, *306*, 245–253.
- [66] J. Rosen, G. S. Hutchings, Q. Lu, R. V. Forest, A. Moore, F. Jiao, *ACS Catal.* **2015**, *5*, 4586–4591.
- [67] Q. Lu, J. Rosen, Y. Zhou, G. S. Hutchings, Y. C. Kimmel, J. G. Chen, F. Jiao, *Nat. Commun.* **2014**, *5*, 3242–3247.
- [68] Y. Yoon, A. S. Hall, Y. Surendranath, *Angew. Chem. Int. Ed.* **2016**, *55*, 15282–15286; *Angew. Chem.* **2016**, *128*, 15508–15512.
- [69] M. Ma, B. J. Trzesniewski, J. Xie, W. A. Smith, *Angew. Chem. Int. Ed.* **2016**, *55*, 9748–9752; *Angew. Chem.* **2016**, *128*, 9900–9904.
- [70] Y. Chen, M. W. Kanan, *J. Am. Chem. Soc.* **2012**, *134*, 1986–1989.
- [71] S. Zhao, S. Li, T. Guo, S. Zhang, J. Wang, Y. Wu, Y. Chen, *Nano-Micro Lett.* **2019**, *11*, 62.
- [72] R. Zhang, W. Lv, L. Lei, *Appl. Surf. Sci.* **2015**, *356*, 24–29.
- [73] J. Wu, Y. Huang, W. Ye, Y. Li, *Adv. Sci.* **2017**, *4*, 1700194.
- [74] A. Del Castillo, M. Alvarez-Guerra, J. Solla-Gullón, A. Sáez, V. Montiel, A. Irabien, *J. CO<sub>2</sub> Util.* **2017**, *18*, 222–228.
- [75] J. Wu, P. P. Sharma, B. H. Harris, X. D. Zhou, *J. Power Sources* **2014**, *258*, 189–194.
- [76] J. Albo, A. Sáez, J. Solla-Gullón, V. Montiel, A. Irabien, *Appl. Catal. B* **2015**, *176–177*, 709–717.
- [77] T. Kottakkat, K. Klingan, S. Jiang, Z. P. Jovanov, V. H. Davies, G. A. M. El-Nagar, H. Dau, C. Roth, *ACS Appl. Mater. Interfaces* **2019**, *11*, 14734–14744.
- [78] X. She, T. Zhang, Z. Li, H. Li, H. Xu, J. Wu, *Cell Rep. Phys. Sci.* **2020**, *1*, 100051.
- [79] C. Li, G. Shen, R. Zhang, D. Wu, C. Zou, T. Ling, H. Liu, C. Dong, X.-W. Du, *J. Mater. Chem. A* **2019**, *7*, 1418–1423.
- [80] A. Dhakshinamoorthy, S. Navalon, A. Corma, H. Garcia, *Energy Environ. Sci.* **2012**, *5*, 9217–9233.
- [81] Y. Li, W.-N. Wang, Z. Zhan, M.-H. Woo, C.-Y. Wu, P. Biswas, *Appl. Catal. B* **2010**, *100*, 386–392.
- [82] S. C. Ma, Y. C. Lan, G. M. J. Perez, S. Moniri, P. J. A. Kenis, *ChemSusChem* **2014**, *7*, 866–874.
- [83] M. A. Farkhondehfar, S. Hernández, M. Rattalino, M. Makkee, A. Lambert, A. Chiodoni, K. Bejtka, A. Sacco, F. C. Pirri, N. Russo, *Int. J. Hydrogen Energy* **2020**, *45*, 26458–26471.
- [84] J. Qu, X. Zhang, Y. Wang, C. Xie, *Electrochim. Acta* **2005**, *50*, 3576–3580.
- [85] G. K. Ramesha, J. F. Brennecke, P. V. Kamat, *ACS Catal.* **2014**, *4*, 3249–3254.
- [86] N. E. Mendieta-Reyes, W. Cheuquepán, A. Rodes, R. Gómez, *ACS Catal.* **2020**, *10*, 103–113.
- [87] P. Jeanty, C. Scherer, E. Magori, K. Wiesner-Fleischer, O. Hinrichsen, M. Fleischer, *J. CO<sub>2</sub> Util.* **2018**, *24*, 454–462.
- [88] S. Hernandez-Aldave, E. Andreoli, *Catalysts* **2020**, *10*, 713.
- [89] L. Weng, A. T. Bell, A. Z. Weber, *Phys. Chem. Chem. Phys.* **2018**, *20*, 16973–16984.
- [90] Q. Wang, H. Dong, H. Yu, *J. Power Sources* **2014**, *271*, 278–284.
- [91] W. Luo, J. Zhang, M. Li, A. Züttel, *ACS Catal.* **2019**, *9*, 3783–3791.
- [92] R. L. Machunda, H. Ju, J. Lee, *Curr. Appl. Phys.* **2011**, *11*, 986–988.
- [93] Y.-J. Zhang, V. Sethuraman, R. Michalsky, A. A. Peterson, *ACS Catal.* **2014**, *4*, 3742–3748.
- [94] S. Back, M. S. Yeom, Y. Jung, *ACS Catal.* **2015**, *5*, 5089–5096.
- [95] M. Valenti, N. P. Prasad, R. Kas, D. Bohra, M. Ma, V. Balasubramanian, L. Chu, S. Gimenez, J. Bisquert, B. Dam, W. A. Smith, *ACS Catal.* **2019**, *9*, 3527–3536.

- [96] A. Goyal, G. Marcandalli, V. A. Mints, M. T. M. Koper, *J. Am. Chem. Soc.* **2020**, *142*, 4154–4161.
- [97] D. W. Dewulf, A. J. Bard, *Catal. Lett.* **1988**, *1*, 73–80.
- [98] L. M. Aeshala, S. U. Rahman, A. Verma, *Sep. Purif. Technol.* **2012**, *94*, 131–137.
- [99] L. M. Aeshala, R. Uppaluri, A. Verma, *Phys. Chem. Chem. Phys.* **2014**, *16*, 17588–17594.
- [100] M. König, J. Vaes, E. Klemm, D. Pant, *iScience* **2019**, *19*, 135–160.
- [101] T. C. Berto, L. Zhang, R. J. Hamers, J. F. Berry, *ACS Catal.* **2015**, *5*, 703–707.
- [102] E. E. L. Tanner, C. Batchelor-McAuley, R. G. Compton, *J. Phys. Chem. C* **2016**, *120*, 26442–26447.
- [103] A. Schizodimou, G. Kyriacou, *Electrochim. Acta* **2012**, *78*, 171–176.
- [104] M. Dunwell, Q. Lu, J. M. Heyes, J. Rosen, J. G. Chen, Y. Yan, F. Jiao, B. Xu, *J. Am. Chem. Soc.* **2017**, *139*, 3774–3783.
- [105] K. Ogura, J. R. Ferrell, A. V. Cugini, E. S. Smotkin, M. D. Salazar-Villalpando, *Electrochim. Acta* **2010**, *56*, 381–386.
- [106] A. S. Varela, W. Ju, T. Reier, P. Strasser, *ACS Catal.* **2016**, *6*, 2136–2144.
- [107] J. Resasco, Y. Lum, E. Clark, J. Z. Zeddon, A. T. Bell, *ChemElectroChem* **2018**, *5*, 1064–1072.
- [108] S. Hong, S. Lee, S. Kim, J. Kwang Lee, J. Lee, *Catal. Today* **2017**, *295*, 82–88.
- [109] A. Díaz-Duque, A. P. Sandoval-Rojas, A. F. Molina-Osorio, J. M. Feliu, M. F. Suárez-Herrera, *Electrochem. Commun.* **2015**, *61*, 74–77.
- [110] A. E. Rudnev, U. E. Zhumaev, A. Kuzume, S. Vesztergom, J. Furrer, P. Broekmann, T. Wandlowski, *Electrochim. Acta* **2016**, *189*, 38–44.
- [111] Y. Tomita, S. Teruya, O. Koga, Y. Hori, *J. Electrochem. Soc.* **2000**, *147*, 4164–4167.
- [112] E. Lamy, L. Nadjo, J. M. Saveant, *J. Electroanal. Chem. Interfacial Electrochem.* **1977**, *78*, 403–407.
- [113] M. C. Figueiredo, I. Ledezma-Yanez, M. T. M. Koper, *ACS Catal.* **2016**, *6*, 2382–2392.
- [114] J. Shi, F. X. Shen, F. Shi, N. Song, Y. J. Jia, Y. Q. Hu, Q. Y. Li, J. X. Liu, T. Y. Chen, Y. N. Dai, *Electrochim. Acta* **2017**, *240*, 114–121.
- [115] J. Lee, D. C. Sorescu, X. Deng, *J. Am. Chem. Soc.* **2011**, *133*, 10066–10069.
- [116] S. M. Aliwi, K. F. Al-Jubori, *Sol. Energy Mater.* **1989**, *18*, 223–229.
- [117] Z. Goren, I. Willner, A. J. Nelson, A. J. Frank, *J. Phys. Chem.* **1990**, *94*, 3784–3790.
- [118] M. M. Taqui Khan, N. Nageswara Rao, D. Chatterjee, *J. Photochem. Photobiol. A* **1991**, *60*, 311–318.
- [119] M. Anpo, K. Chiba, *J. Mol. Catal.* **1992**, *74*, 207–212.
- [120] K. Sayama, H. Arakawa, *J. Phys. Chem.* **1993**, *97*, 3, 531–533.
- [121] H. Yamashita, H. Nishiguchi, N. Kamada, M. Anpo, Y. Teraoka, H. Hatano, S. Ehara, K. Kikui, L. Palmisano, A. Sclafani, M. Schiavello, M. A. Fox, *Res. Chem. Intermed.* **1994**, *20*, 815–823.
- [122] K. Adachi, K. Ohta, T. Mizuno, *Sol. Energy* **1994**, *53*, 187–190.
- [123] J. Hou, H. Cheng, O. Takeda, H. Zhu, *Angew. Chem. Int. Ed.* **2015**, *54*, 8480–8484; *Angew. Chem.* **2015**, *127*, 8600–8604.
- [124] S. N. Habisreutinger, L. Schmidt-Mende, J. K. Stolarczyk, *Angew. Chem. Int. Ed.* **2013**, *52*, 7372–7408; *Angew. Chem.* **2013**, *125*, 7516–7557.
- [125] W. Tu, Y. Zhou, Z. Zou, *Adv. Mater.* **2014**, *26*, 4607–4626.
- [126] X. Li, J. Yu, M. Jaroniec, X. Chen, *Chem. Rev.* **2019**, *119*, 3962–4179.
- [127] O. Ola, M. Maroto-Valer, *J. Photochem. Photobiol. C* **2015**, *24*, 16–42.
- [128] J. Low, B. Cheng, J. Yu, *Appl. Surf. Sci.* **2017**, *392*, 658–686.
- [129] H. Abdullah, M. M. R. Khan, H. R. Ong, Zahira Yaako, *J. CO<sub>2</sub> Util.* **2017**, *22*, 15–32.
- [130] M. Bellardita, A. Di Paola, E. García-López, V. Loddò, G. Marci, L. Palmisano, *Curr. Org. Chem.* **2013**, *17*, 2440–2448.
- [131] M. M. Kandy, *Sustain. Energy Fuels* **2020**, *4*, 469–484.
- [132] H. Huang, B. Pradhan, J. Hofkens, M. B. J. Roefsaers, J. A. Steele, *ACS Energy Lett.* **2020**, *5*, 1107–1123.
- [133] R. Liu, Z. Chen, Y. Yao, Y. Li, W. A. Cheema, D. Wang, S. Zhu, *RSC Adv.* **2020**, *10*, 29408–29418.
- [134] P. Prabhu, V. Jose, J.-M. Lee, *Adv. Funct. Mater.* **2020**, *30*, 1910768.
- [135] D. Li, M. Kassymova, X. Cai, S.-Q. Zang, H.-L. Jiang, *Coord. Chem. Rev.* **2020**, *412*, 213262.
- [136] B. Di Credico, M. Redaelli, M. Bellardita, M. Calamante, C. Cepek, E. Cobani, M. D'Arienzo, C. Evangelisti, M. Marelli, M. Moret, L. Palmisano, *R. Scotti Catalysis* **2018**, *8*, 353.
- [137] S. Al Jitan, G. Palmisano, C. Garlisi, *Catalysts* **2020**, *10*, 227.
- [138] G. R. Dey, A. D. Belapurkar, K. Kishore, *J. Photochem. Photobiol. A* **2004**, *163*, 503–508.
- [139] S. S. Tan, L. Zou, E. Hu, *Catal. Today* **2006**, *115*, 269–273.
- [140] J. Fu, S. Cao, J. Yu, J. Low, Y. Lei, *Dalton Trans.* **2014**, *43*, 9158–9165.
- [141] K. Kočí, L. Obalová, L. Matějová, D. Plachá, Z. Lacný, J. Jirkovský, O. Šolcová, *Appl. Catal. B* **2009**, *89*, 494–502.
- [142] J. Yu, J. Low, W. Xiao, P. Zhou, M. Jaroniec, *J. Am. Chem. Soc.* **2014**, *136*, 8839–8842.
- [143] Z. Lei, Z. Xiong, Y. Wang, Y. Chen, D. Cao, Y. Zhao, J. Zhang, C. Zheng, *Catal. Commun.* **2018**, *108*, 27–32.
- [144] P.-Q. Wang, Y. Bai, J.-Y. Liu, Z. Fan, Y.-Q. Hu, *Catal. Commun.* **2012**, *29*, 185–188.
- [145] G. H. Li, S. Ciston, Z. V. Saponjic, L. Chen, N. M. Dimitrijevic, T. Rajh, K. A. Gray, *J. Catal.* **2008**, *253*, 105–110.
- [146] L. Liu, H. Zhao, J. M. Andino, Y. Li, *ACS Catal.* **2012**, *2*, 1817–1828.
- [147] X. Meng, S. Ouyang, T. Kako, P. Li, Q. Yu, T. Wang, J. Ye, *Chem. Commun.* **2014**, *50*, 11517–11519.
- [148] K. Adachi, K. Ohta, T. Mizuno, *Sol. Energy* **1994**, *53*, 187–190.
- [149] Slamet, H. W. Nasution, E. Purnama, S. Kosela, J. Gunlazuardi, *Catal. Commun.* **2005**, *6*, 313–319.
- [150] L. Liu, F. Gao, H. Zhao, Y. Li, *Appl. Catal. B* **2013**, *134*, 349–358.
- [151] L.-H. Tseng, J. C.-S. Wu, *Catal. Today* **2004**, *97*, 113–119.
- [152] D. Liu, Y. Fernández, O. Ola, S. Mackintosh, M. Maroto-Valer, C. M. A. Parlett, A. F. Lee, J. C. S. Wu, *Catal. Commun.* **2012**, *25*, 78–82.
- [153] M. Sellaro, M. Bellardita, A. Brunetti, E. Fontananova, L. Palmisano, E. Drioli, G. Barbieri, *RSC Adv.* **2016**, *6*, 67418–67427.
- [154] L. Liu, C. Zhao, Y. Li, *J. Phys. Chem. C* **2012**, *116*, 7904–7912.
- [155] S.-M. Park, A. Razaq, Y. H. Park, S. Sorcar, Y. Park, C. A. Grimes, S.-I. In, *ACS Omega* **2016**, *1*, 868–875.
- [156] W.-N. Wang, W.-J. An, B. Ramalingam, S. Mukherjee, D. M. Niedzwiedzki, S. Gangopadhyay, P. Biswas, *J. Am. Chem. Soc.* **2012**, *134*, 11276–11281.
- [157] L. Qiu-ye, Z. Lan-lan, L. Chen, C. Yu-hui, W. Xiao-dong, Y. Jian-jun, *Adv. Condens. Matter Phys.* **2014**, ID 316589.
- [158] M. Tasbihi, Kamila Kočí, M. Edelmánová, I. Troppová, M. Reli, R. Schomäcker, *J. Photochem. Photobiol. A* **2018**, *366*, 72–80.
- [159] Y. Wang, Q. Lai, F. Zhang, X. Shen, M. Fan, Y. He, S. Ren, *RSC Adv.* **2014**, *4*, 44442–44451.
- [160] X. Zhang, F. Han, B. Shi, S. Farsinezhad, P. Dechaine, G. K. Shankar, *Angew. Chem. Int. Ed.* **2012**, *51*, 12732–12735; *Angew. Chem.* **2012**, *124*, 12904–12907.
- [161] Q. Zhai, S. Xie, W. Fan, Q. Zhang, Y. Wang, W. Deng, Y. Wang, *Angew. Chem. Int. Ed.* **2013**, *52*, 5776.
- [162] W. Hou, W. H. Hung, P. Pavaskar, A. Goeppert, M. Aykol, S. B. Cronin, *ACS Catal.* **2011**, *1*, 929–936.
- [163] X. Li, Z. Zhuang, W. Li, H. Pan, *Appl. Catal. A* **2012**, *429–430*, 31–38.
- [164] M. Tahir, N. S. Amin, *Appl. Catal. B* **2015**, *162*, 98–109.
- [165] E. Liu, L. Kang, F. Wu, T. Sun, X. Hu, Y. Yang, H. Liu, J. Fan, *Plasmonics* **2014**, *9*, 61–70.
- [166] K. Li, T. Peng, Z. Ying, S. Song, J. Zhang, *Appl. Catal. B* **2016**, *180*, 130–138.
- [167] S. Xie, Y. Wang, Q. Zhang, W. Deng, Y. Wang, *ACS Catal.* **2014**, *4*, 3644–3653.
- [168] Y. G. Wang, B. Li, C. L. Zhang, L. F. Cui, S. F. Kang, X. Li, L. H. Zhou, *Appl. Catal. B* **2013**, *130*, 277–284.
- [169] S. Neatu, J. A. Maciá-Agulló, P. Concepcion, H. Garcia, *J. Am. Chem. Soc.* **2014**, *136*, 15969–15976.
- [170] S. Zhu, W. Liao, M. Zhang, S. Liang, *Chem. Eng. J.* **2019**, *361*, 461–469.
- [171] Y. G. Wang, F. Wang, Y. Chen, D. Zhang, B. Li, S. Kang, X. Li, L. Cui, *Appl. Catal. B* **2014**, *147*, 602–609.
- [172] X. Y. Chen, Y. Zhou, Q. Liu, Z. D. Li, J. G. Liu, Z. G. Zou, *ACS Appl. Mater. Interfaces* **2012**, *4*, 3372–3377.
- [173] L. Zhang, C. Xie, H. Jiu, Y. Meng, Q. Zhang, Y. Gao, *Catal. Lett.* **2018**, *148*, 2812–2821.
- [174] M. Reli, P. Huo, M. Šihor, N. Ambrožová, I. Troppová, L. Matějová, J. Lang, L. Svoboda, P. Kušrowski, M. Ritz, P. Praus, K. Kočí, *J. Phys. Chem. A* **2016**, *120*, 8564–8573.
- [175] Y. He, L. Zhang, B. Teng, M. Fan, *Environ. Sci. Technol.* **2014**, *49*, 649–656.
- [176] K. Kočí, K. Zatloukalová, L. Obalová, S. Krejčíková, Z. Lacný, L. Čapek, A. Hospodková, O. Šolcová, *Chin. J. Catal.* **2011**, *32*, 812–815.
- [177] C.-C. Yang, Y.-H. Yu, B. van der Linden, J. C. S. Wu, G. Mul, *J. Am. Chem. Soc.* **2010**, *132*, 8399–8406.
- [178] B. Mei, A. Pougin, J. Strunk, *J. Catal.* **2013**, *306*, 184–189.
- [179] M. Anpo, *J. CO<sub>2</sub> Util.* **2013**, *1*, 8–17.
- [180] N. Ulagappan, H. Frei, *J. Phys. Chem. A* **2000**, *104*, 7834–7839.
- [181] A. Di Paola, E. García-López, G. Marci, Cristina Martín, L. Palmisano, V. Rives, A. M. Venezia, *Appl. Catal. B* **2004**, *48*, 223–233.



- [182] Y. Liao, S. W. Cao, Y. Yuan, Q. Gu, Z. Zhang, C. Xue, *Chem. Eur. J.* **2014**, *20*, 10220–10222.
- [183] S. Liu, J. Xia, J. Yu, *ACS Appl. Mater. Interfaces* **2015**, *7*, 8166–8175.
- [184] J. Zhao, Y. Wang, Y. Li, X. Yue, C. Wang, *Catal. Sci. Technol.* **2016**, *6*, 7967–7975.
- [185] J. Guo, S. Ouyang, T. Kako, J. Ye, *Appl. Surf. Sci.* **2013**, *280*, 418–423.
- [186] G. Busca, *Catal. Today* **1998**, *41*, 191–206.
- [187] W. Tu, Y. Zhou, Z. Zou, *Adv. Mater.* **2014**, *26*, 4607–4626.
- [188] R. Liu, Z. Chen, Y. Yao, Y. Li, W. A. Cheema, D. Wang, S. Zhu, *RSC Adv.* **2020**, *10*, 29408–29418.
- [189] D. M. S. Marcolongo, F. Nocito, N. Ditaranto, M. Aresta, A. Dibenedetto, *Catalysts* **2020**, *10*, 980.
- [190] Y. Bo, Chao Gao, Y. Xiong, *Nanoscale* **2020**, *12*, 12196–12209.
- [191] Z. Wang, S. A. Monny, L. Wang, *ChemNanoMat* **2020**, *6*, 881–888.
- [192] S. Huygh, A. Bogaerts, E. C. Neyts, *J. Phys. Chem. C* **2016**, *120*, 21659–21669.
- [193] Y. Zhang, C. Xu, J. Chen, X. Zhang, Z. Wang, J. Zhou, K. Cen, *Appl. Energy* **2015**, *156*, 223–229.
- [194] J. Lee, D. C. Sorescu, X. Deng, *J. Am. Chem. Soc.* **2011**, *133*, 10066–10069.
- [195] H. Metiu, S. Chrétien, Z. Hu, B. Li, X. Sun, *J. Phys. Chem. C* **2012**, *116*, 10439–10450.
- [196] M. Bellardita, C. Garlisi, L. Y. Ozer, A. M. Venezia, J. Sá, F. Mamedov, L. Palmisano, G. Palmisano, *Appl. Surf. Sci.* **2020**, *510*, 145419.
- [197] K. Li, X. An, K. H. Park, M. Khraisheh, J. Tang, *Catal. Today* **2014**, *224*, 3–12.
- [198] S. Gao, B. Gu, X. Jiao, Y. Sun, X. Zu, F. Yang, W. Zhu, C. Wang, Z. Feng, B. Ye, Y. Xie, *J. Am. Chem. Soc.* **2017**, *139*, 3438–3445.
- [199] A. Iwase, S. Yoshino, T. Takayama, Y. H. Ng, R. Amal, A. Kudo, *J. Am. Chem. Soc.* **2016**, *138*, 10260–10264.
- [200] S. Yan, H. Yu, N. Wang, Z. Li, Z. Zou, *Chem. Commun.* **2012**, *48*, 1048–1050.
- [201] Q. Kang, T. Wang, P. Li, L. Liu, K. Chang, M. Li, J. Ye, *Angew. Chem. Int. Ed.* **2015**, *54*, 841–845; *Angew. Chem.* **2015**, *127*, 855–859.
- [202] J. Chen, S. Qin, G. Song, T. Xiang, F. Xin, X. Yin, *Dalton Trans.* **2013**, *42*, 15133–15138.
- [203] K. Teramura, S. Iguchi, Y. Mizuno, T. Shishido, T. Tanaka, *Angew. Chem. Int. Ed.* **2012**, *124*, 8132–8135.
- [204] B. Al Otaibi, X. Kong, S. Vanka, S. Y. Woo, A. Pofelski, F. Oudjedi, S. Fan, M. G. Kibria, G. A. Botton, W. Ji, H. Guo, Z. Mi, *ACS Energy Lett.* **2016**, *1*, 246–252.
- [205] M. Bellardita, V. Augugliaro, V. Loddo, B. Megna, G. Palmisano, L. Palmisano, M. A. Puma, *Appl. Catal. A* **2012**, *441–442*, 79–89.
- [206] E. Kalamaras, M. M. Maroto-Valer, M. Shao, J. Xuan, H. Wang, *Catal. Today* **2018**, *317*, 56–75.
- [207] S. Xie, Q. Zhang, G. Liu, Y. Wang, *Chem. Commun.* **2016**, *52*, 35–59.
- [208] M. Halman, *Nature* **1978**, *275*, 115–116.
- [209] T. Arai, S. Sato, K. Uemura, T. Morikawa, T. Kajino, *Chem. Commun.* **2010**, *46*, 6944–6946.
- [210] T. Arai, S. Tajima, S. Sato, K. Uemura, T. Morikawa, T. Kajino, *Chem. Commun.* **2011**, *47*, 12664–12666.
- [211] B. Kumar, J. M. Smieja, A. F. Sasayama, C. P. Kubiak, *Chem. Commun.* **2012**, *48*, 272–274.
- [212] M. Schreier, P. Gao, M. T. Mayer, J. Luo, T. Moehl, M. K. Nazeeruddin, S. D. Tilley, M. Grätzel, *Energy Environ. Sci.* **2015**, *8*, 855–861.
- [213] Y. Kou, S. Nakatani, G. Sunagawa, Y. Tachikawa, D. Masui, T. Shimada, S. Takagi, D. A. Tryk, Y. Nabetani, H. Tachibana, H. Inoue, *J. Catal.* **2014**, *310*, 57–66.
- [214] G. Sahara, R. Abe, M. Higashi, T. Morikawa, K. Maeda, Y. Ueda, O. Ishitani, *Chem. Commun.* **2015**, *51*, 10722–10725.
- [215] D. H. Won, J. Chung, S. H. Park, E. H. Kim, S. I. Woo, *J. Mater. Chem. A* **2015**, *3*, 1089–1095.
- [216] J. Jang, S. Cho, G. Magesh, Y. Jang, J. Kim, W. Kim, J. Seo, S. Kim, K. Lee, J. Lee, *Angew. Chem. Int. Ed.* **2014**, *53*, 5852–5857; *Angew. Chem.* **2014**, *126*, 5962–5967.
- [217] A. T. Garcia-Esparza, K. Limkraisiri, F. Leroy, S. Rasul, W. Yu, L. Lin, K. Takanabe, *J. Mater. Chem. A* **2014**, *2*, 7389–7401.
- [218] D. Won, C. Choi, J. Chung, S. Woo, *Appl. Catal. B* **2014**, *158–159*, 217–223.
- [219] J. F. de Brito, A. Araujo, K. Rajeshwa, M. Zanoni, *Chem. Eng. J.* **2015**, *264*, 302–309.
- [220] Q. Shen, Z. Chen, X. Huang, M. Liu, G. Zhao, *Environ. Sci. Technol.* **2015**, *49*, 5828–5835.
- [221] U. Kang, S. K. Choi, D. J. Ham, S. M. Ji, W. Choi, D. S. Han, A. Abdel-Wahab, H. Park, *Energy Environ. Sci.* **2015**, *8*, 2638–2643.
- [222] J. Gu, A. Wuttig, J. W. Krizan, Y. Hu, Z. M. Detweiler, R. J. Cava, A. B. Bocarsly, *J. Phys. Chem. C* **2013**, *117*, 12415–12422.
- [223] P. Li, H. Hu, J. Xu, H. Jing, H. Peng, J. Lu, C. Wu, S. Ai, *Appl. Catal. B* **2014**, *147*, 912–919.
- [224] S. Xia, Y. Menga, X. Zhou, J. Xue, G. Pan, Z. Ni, *Appl. Catal. B* **2016**, *187*, 122–133.
- [225] T. Tasso Guaraldo, J. Ferreira de Brito, D. Wood, M. V. Boldrin Zanonia, *Electrochim. Acta* **2015**, *185*, 117–124.
- [226] J. Cheng, M. Zhang, G. Wu, X. Wang, J. Zhou, K. Cen, *Sol. Energy Mater. Sol. Cells* **2015**, *132*, 606–614.
- [227] J. A. Lima Perini, J. C. Cardoso, J. F. de Brito, M. V. Boldrin Zanoni, *J. CO<sub>2</sub> Util.* **2018**, *25*, 254–263.
- [228] G. Magesh, E. S. Kim, H. J. Kang, M. Banu, J. Y. Kim, J. H. Kim, J. S. Lee, *J. Mater. Chem. A* **2014**, *2*, 2044–2049.
- [229] S. Sato, T. Arai, T. Morokawa, K. Uemura, T. M. Suzuki, H. Tanaka, T. Kajino, *J. Am. Chem. Soc.* **2011**, *133*, 15240–15243.
- [230] T. Arai, S. Sato, T. Kajino, T. Morikawa, *Energy Environ. Sci.* **2013**, *6*, 1274–1282.
- [231] A. Paracchino, V. Laporte, K. Sivula, M. Grätzel, E. Thimsen, *Nat. Mater.* **2011**, *10*, 456–461.
- [232] G. Panzeri, M. Cristina, M. S. Jagadeesh, G. Bussetti, L. Magagnin, *Sci. Rep.* **2020**, *10*, 18730.
- [233] D. Won, C. Choi, J. Chung, S. Woo, *Appl. Catal. B* **2014**, *158–159*, 217–223.
- [234] X. Huang, T. Cao, M. Liu, G. Zhao, *J. Phys. Chem. C* **2013**, *117*, 26432–26440.
- [235] K. R. Karim, H. R. Ong, H. Abdullah, A. Yousuf, C. K. Cheng, M. R. Khan, *Int. J. Hydrogen Energy* **2018**, *43*, 18185–18193.
- [236] P. Li, X. Sui, J. Xu, H. Jing, C. Wu, H. Peng, J. Lu, H. Yin, *Chem. Eng. J.* **2014**, *247*, 25–32.

Manuscript received: February 9, 2021  
Revised manuscript received: March 29, 2021  
Accepted manuscript online: April 11, 2021  
Version of record online: June 8, 2021